Article:

Bell, D, Kane, IA, Ponten, ASM et al. (3 more authors) (2018) Spatial variability in depositional reservoir quality of deep-water channel-fill and lobe deposits. Marine and Petroleum Geology, 98. pp. 97-115. ISSN 0264-8172

https://doi.org/10.1016/j.marpetgeo.2018.07.023

Spatial variability in depositional reservoir quality of deep-water channel-fill and lobe deposits

Daniel Bell[1*], Ian A. Kane[1], Anna S. M. Pontén[2], Stephen S. Flint[3], David M. Hodgson[4] and Bonita J. Barrett[4]

[1] SedRESQ, School of Earth and Environmental Sciences, University of Manchester, Manchester, M13 9PL, U.K.

[2] Equinor ASA, Research Center Rotvoll, NO-7005 Trondheim, Norway

[3] Stratigraphy Group, School of Earth and Environmental Sciences, University of Manchester, Manchester, M13 9PL, U.K.

[4] Stratigraphy Group, School of Earth and Environment, University of Leeds, Leeds, LS2 9JT, U.K

Email: daniel.bell-2@manchester.ac.uk

Keywords: deep-water sedimentology, reservoir quality, turbidites, submarine channel, submarine lobe, Pyrenees, process sedimentology, sedimentary petrology

Abstract

Initial porosity and permeability in deep-water systems is controlled by primary sedimentary texture and mineralogy. Therefore, understanding the sedimentary processes that control changes in primary texture is critical for improved reservoir quality predictions. A well-constrained, exhumed submarine lobe in the Jaca Basin, and a submarine channel-fill element in the Aínsa Basin, northern Spain, were studied to characterize the depositional reservoir quality in axial to marginal/fringe positions. Construction of architectural panels and strategic sampling enabled analysis of the spatial changes in textural properties, and their relationship to reservoir quality distribution. Samples were analysed in thin-section to establish how depositional processes inferred from outcrop observations affect textural properties. Results show that high-density turbidites are concentrated in lobe- and channel-axis positions and exhibit good depositional reservoir quality. Lobe off-axis deposits contain high- and low-density turbidites and have moderate depositional reservoir quality. Conversely, low-density turbidites dominate lobe fringe and channel-margin positions and have relatively poor depositional reservoir quality. There is a sharp decrease in depositional reservoir quality between the lobe off-axis and lobe fringe due to: 1) an abrupt increase in matrix content; 2) an abrupt decrease in sandstone amalgamation; and 3) a decrease in grain-size. There is an abrupt increase in depositional reservoir quality from channel margin to channel axis corresponding to: 1) an increase in total sandstone thickness and amalgamation; 2) an increase in grain-size, 3) a decrease in matrix content. Rates of change of key properties are up to two orders of magnitude greater between channel-fill sub-environments compared to lobe sub-environments. Spatial variability in properties of discrete architectural elements, and rates of changes, provides input to reservoir models during exploration, appraisal, and development phases of hydrocarbon fields.

1.1 Introduction

Submarine fans represent large volumes of terrigenous sediment transported from the continental shelf to the slope and basin floor (e.g. Emmel and Curray, 1983; Piper et al., 1999; Talling et al., 2007; Prélat et al., 2010; Clare et al., 2014). Modern deep-marine systems are repositories for anthropogenically derived sediment and pollutants, and organic matter (e.g. Galy et al., 2007; Saller et al., 2008; Hodgson, 2009; Gwiazda et al., 2015), and buried systems form reservoirs for groundwater and hydrocarbons, as well as economic accumulations of minerals (e.g. Pettingill, 1998; Ruffell et al., 1998; Weimer et al., 2000; McKie et al., 2015). Consequently, understanding the distribution of depositional facies and their porosity and permeability is key to understanding the distribution and stability of subsurface fluids and minerals (Lien et al., 2006; Porten et al., 2016; Southern et al., 2017).

The porosity of unconsolidated sediments is controlled by the grain-size, sorting and packing of grains (Fraser, 1935; Beard and Weyl, 1973; Hirst et al., 2002; Lien et al., 2006; Njoku and Pirmez, 2011; Porten et al., 2016), whereas detrital clay content, clay mineralogy, and clay distribution have a strong control on permeability (e.g. Wilson, 1992; Hirst et al., 2002; Lien et al., 2006; Ajdukiewicz et al., 2010; Dowey et al., 2012; Porten et al., 2016). These relationships are demonstrated in terrestrial and shallow-marine deposits (e.g. Pryor, 1973; Haile et al., 2017). However, the general inaccessibility of modern deep-water systems means the primary distribution of their textural characteristics is less-well understood.

Controls on reservoir quality operate on a range of scales. At the largest-scale, sandstone reservoir quality is determined by the volume of the deposit and connectivity, as elements include both sand and non-sand reservoir (e.g. Kerr and Jirik, 1990; Hardage et al., 1996; Afifi, 2005; Jolley et al., 2010; Kilhams et al., 2015; Lan et al., 2016). Within the sandstone portion of the reservoir, 'quality' is predominantly determined by grain-scale porosity and permeability (e.g. Fraser, 1935; Marzano, 1988; Ramm and Bjørlykke, 1994; Ehrenberg, 1997; Worden et al., 2000; Marchand et al., 2015; Porten et al., 2016), which is modified by eodiagenetic and mesodiagenetic processes (e.g. Ehrenberg, 1989; Pittman and Larese, 1991; Ramm and Bjørlykke, 1994; Ehrenberg, 1997; Worden et al., 2000). It is recognized that the primary texture of depositional facies in deep-water sandstones can also maintain a strong control even after diagenesis (Hirst et al., 2002; Lien et al., 2006; Njoku and Pirmez, 2011; Kilhams et al., 2012; Marchand et al., 2015; Porten et al., 2016). "Depositional reservoir quality" is the initial reservoir potential of a sedimentary accumulation prior to post-depositional modification (Porten et al., 2016). The type of flow that generates a deposit has a strong influence on its texture (Hirst et al., 2002; Lien et al., 2006; Njoku and Pirmez, 2011; Kilhams et al., 2012; Porten et al., 2016; Kane et al., 2017). Therefore, the primary texture of deposits from discrete flow-types can also maintain a strong control during all stages of diagenesis (Hirst et al., 2002; Lien et al., 2006; Njoku and Pirmez, 2011; Kilhams et al., 2012; Marchand et al., 2015; Porten et al., 2016).

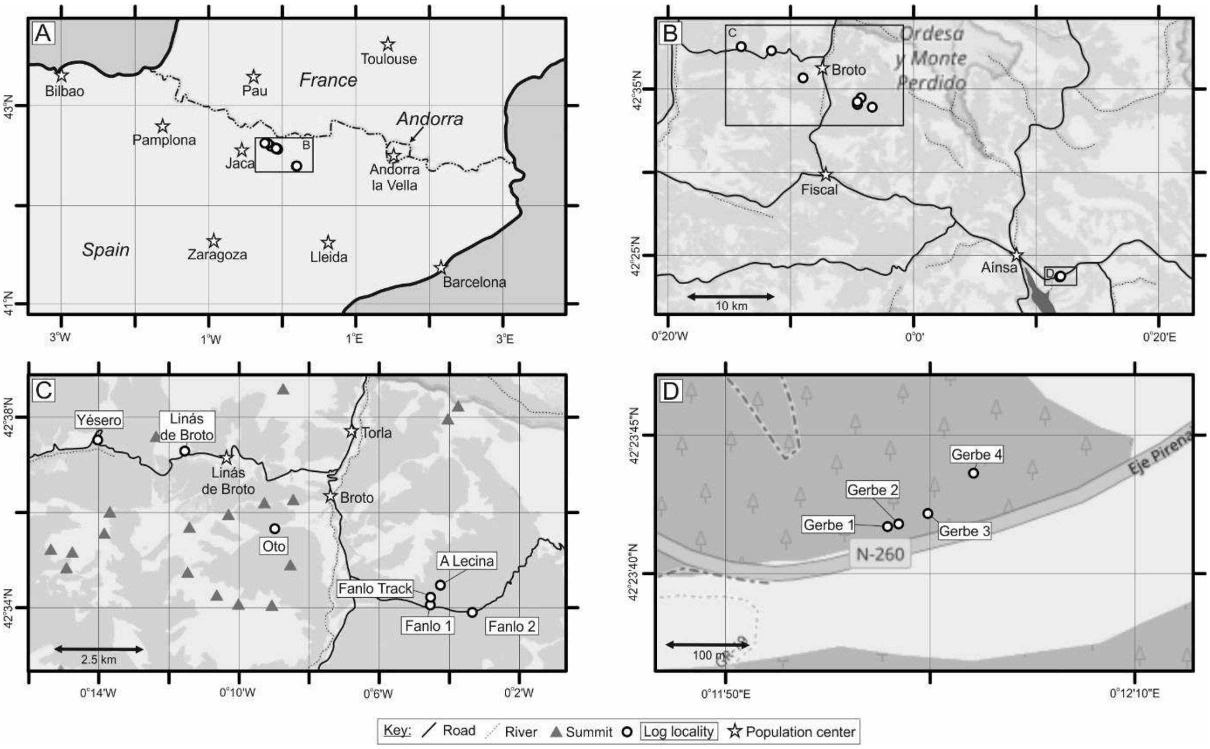

Figure 1: A) Location of study area in Spain; B) Regional locality map showing the two studied areas; C) Localities of the Gerbe channel-fill outcrops; D) Localities of Upper Broto, Lobe 1 outcrops. Image sources: Esri, DeLorme, HERE, MapmyIndia, OpenStreetMap contributors.

Deep-water systems consist of depositional elements, which are hierarchically organized (e.g. Mutti and Ricci-Lucchi, 1972; Mutti, 1985; Mutti and Normark, 1987; Clark and Pickering, 1996; Sprague et al., 2002; Deptuck et al., 2008; Prélat et al., 2009; Di Celma et al., 2011), the organization of which controls the overall size and connectivity of a reservoir. Architectural elements are determined by their size, architecture, bounding surfaces, and relationship to other architectural elements (e.g. Miall, 1985; Mutti and Normark, 1987; Clark and Pickering, 1996; Sprague et al., 2002; Prélat et al., 2009). Individual depositional facies have variable grain-scale textures, and therefore the spatial arrangement of these depositional facies within an architectural element will determine reservoir potential distribution at that hierarchical level. The stacking of architectural elements and their inherited grain-scale texture allows prediction of reservoir quality at higher levels in the architectural hierarchy. Therefore, understanding facies distribution and grain-scale character is critical to improved prediction of reservoir distribution. Previous publications related to the integration of architectural- and grain-scale observations typically consider broad proximal-to-distal trends, or consider facies variability with limited spatial control (Hirst et al., 2002; Lien et al., 2006; Njoku and Pirmez, 2011; Kilhams et al., 2012; Marchand et al., 2015; Porten et al., 2016). Geochemical and mineralogical variations have been recognized within a deep-water channel complex and attributed to the primary texture (Aehnelt et al., 2013). However, no published work has attempted to constrain the depositional reservoir quality within a single architectural element. To assess this issue the following research questions will be addressed: 1) How can an architectural element be characterized at grain-scale? 2) How does reservoir potential vary spatially within an individual architectural element? 3) How do sediment gravity flow processes influence depositional reservoir quality and its distribution?

2.1 Geological setting

During the Early Eocene the Aínsa-Jaca Basin developed as an east-west trending, southward migrating foredeep (Puigdefàbregas et al., 1975; Mutti, 1984; Labaume et al., 1985; Mutti, 1985; Mutti et al., 1988; Muñoz, 1992; Teixell and García-Sansegundo, 1995). The deep-water deposits form the Hecho Group (Fig. 2; Mutti, 1985). The Aínsa Basin fill predominantly consists of submarine slope channel systems and mass-transport deposits, separated by marlstones (e.g. Mutti, 1977; Clark et al., 1992; Mutti, 1992; Clark and Pickering, 1996; Remacha et al., 2003; Pickering and Corregidor, 2005; Moody et al., 2012; Dakin et al., 2013; Bayliss and Pickering, 2015). The Gerbe System (Fig. 2) is interpreted as a canyon to lower-slope channel system (Mutti, 1992;

Clark and Pickering, 1996), and consists of: 1) a lower unit that comprizes conglomerate lags, which is interpreted as sediment bypass-dominated; and 2) an upper unit that comprizes fining-upward channel-fill elements and records the aggradation and shutdown of the channel system (Mutti, 1992). This study analyzes one channel-fill element from the upper unit.

The Jaca Basin succession, which is separated from the exposed part of the Aínsa Basin by the Boltaña Anticline, is interpreted as a series of submarine fans, consisting of lobes and basin-plain deposits (Fig. 2; Mutti, 1977; Mutti, 1992; Remacha et al., 2005; Bell et al., *in press*). The stratigraphy of the basin-fill is constrained by nine regionally mapped ‘megabeds’ (Rupke, 1976; Labaume et al., 1987; Rosell and Wiezorek, 1989; Payros et al., 1999).

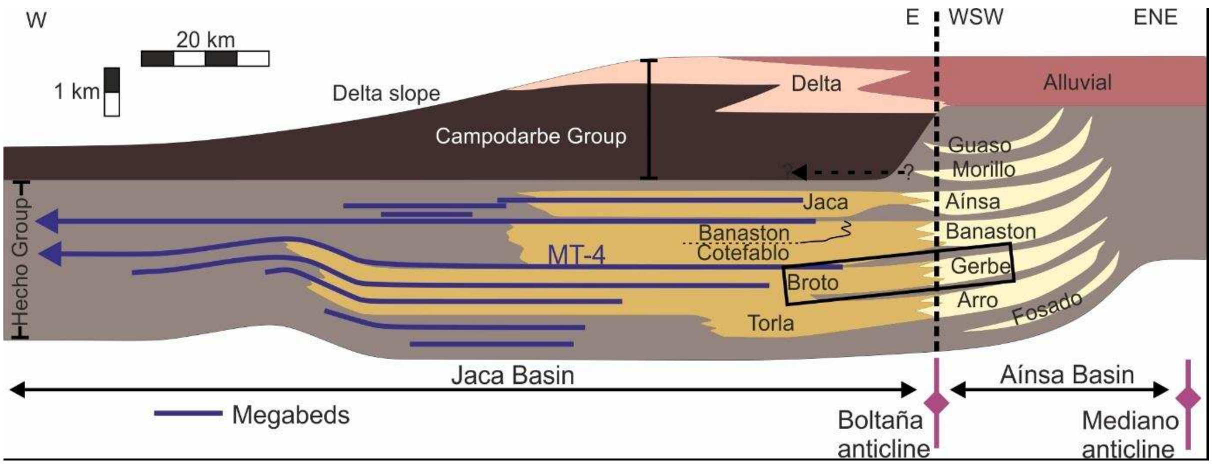

Figure 2: Stratigraphy and geological setting of the Aínsa-Jaca Basin fill. Regional depositional dip is from right to left, with tentative correlation across the Boltaña anticline following Das Gupta and Pickering (2008).

The lobe component of this study focuses on the Upper Broto System, immediately underlying the MT-4 megabed (see also: Mutti, 1992). The Upper Broto is interpreted as proximal lobes (Mutti, 1992; Bell et al., *in press*), with distal hybrid bed dominated packages where depositional architecture is interpreted to have been influenced by topography (Remacha and Fernández, 2003; Remacha et al., 2005 Bell et al. *in press*;).

3.1 Methods

Different stratigraphic correlations between the Aínsa and Jaca Basins have been proposed (Mutti, 1984; Mutti, 1985; Mutti, 1992; Remacha et al., 2003; Das Gupta and Pickering, 2008; Caja et al., 2010; Clark et al., 2017). Following Das Gupta and Pickering (2008), the Gerbe (Aínsa) and Broto (Jaca) Systems are considered as broadly equivalent and are studied here. Whilst uncertainty remains with this correlation, the two systems form part of the genetically related wider basin-fill, have the same burial history, and, for the puposes of this study, are comparable. Furthermore, linked channel-fills and lobes may accumulate diachronously (e.g. Hodgson et al., 2016), and challenges in correlating individual channel-fills with individual lobes at outcrop mean that sampling the exact time-equivalent stratigraphy may not be possible. One channel-fill element and one lobe were selected from the outcrops to be studied in detail. Detailed sedimentary logs and thin-section analysis were used to investigate spatial changes in architecture, facies and grain-scale texture within the channel-fill and lobe.

In the subsurface, reservoir intervals are typically sampled by core plugging at regular intervals, and are biased towards sandstone. These sampling protocols are not designed to capture variability at the architectural element scale. An alternative approach is to sample beds that conform to the mean average bed thickness in an architectural element. However, this would preferentially select thinner beds, which are more common than medium- or thick-bedded sandstone, but typically account for a smaller proportion of the overall sandstone content. Therefore, to characterize an architectural element at grain-scale a repeatable 'stratigraphic sampling' method was developed to sample an 'average' bed characteristic of the sampled succession (Fig. 3). The method is as follows: a logged section through an architectural element was sub-divided into three sections or 'windows' of equal thickness (steps 1 and 2, Fig. 3). Where a window boundary fell within a bed, the boundary was moved to the closest base or top of the nearest sandstone bed. The proportion of sandstone that the thickest and thinnest beds constituted in a window was calculated (step 3, Fig. 3). An average of the two was taken and converted back to a thickness (step 3 Fig. 3). The bed with a thickness that most closely corresponded to this calculated thickness was chosen to be sampled as an 'average bed' for the succession (step 4, Fig. 3). A sample of the selected bed was collected from the center of the bed, to avoid the coarse-grained base or fine-grained top. Sampling was designed to assess sedimentary process controls on the depositional reservoir quality of sandstones within architectural elements. Therefore, the texture of non-reservoir facies (e.g. mudstones) were not studied. However, the effects of these potential barriers to flow are considered in architectural element scale analysis.

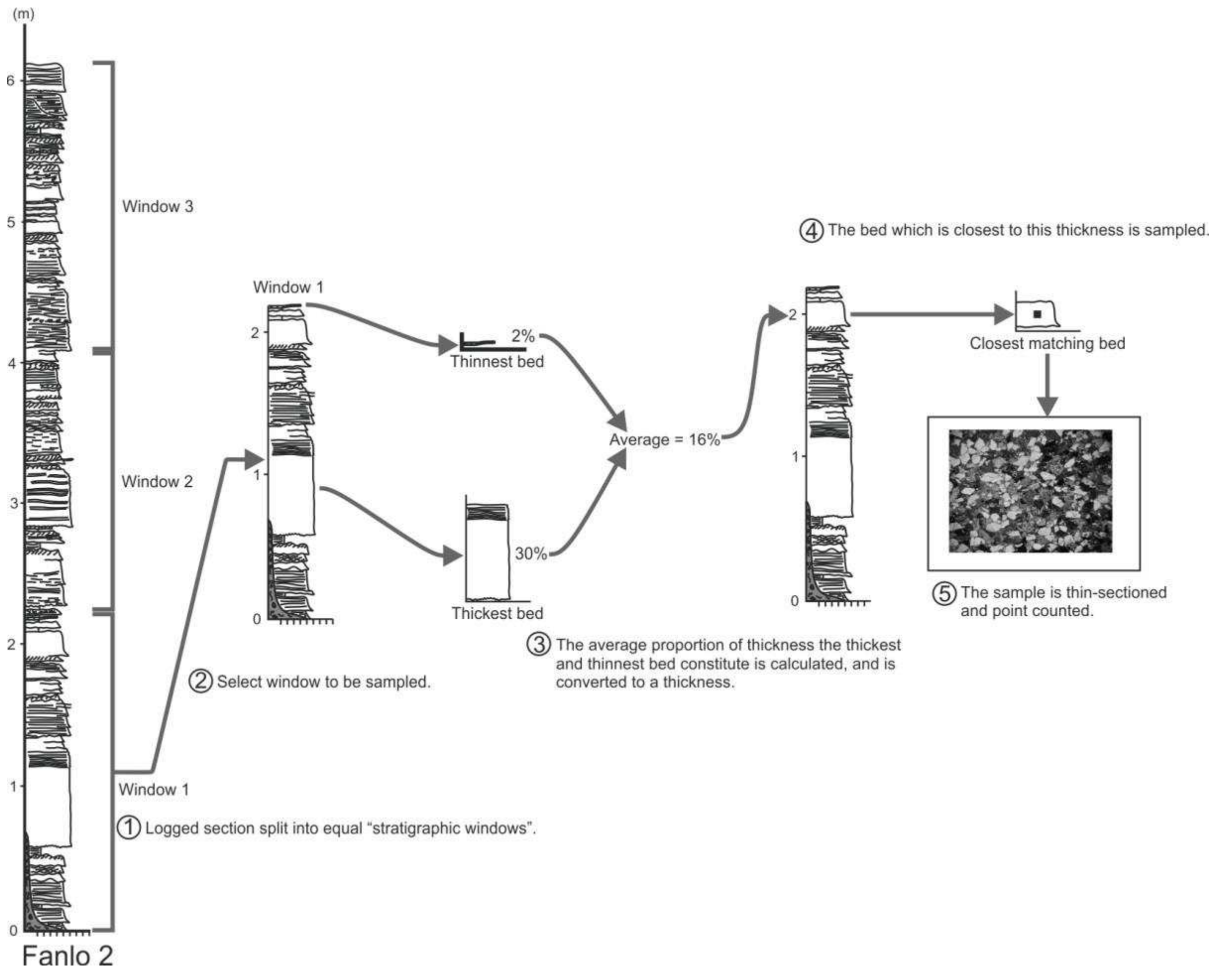

Figure 3: The workflow for a repeatable stratigraphic sampling method. Vertical scale in meters.

Thin-sections were point-counted using a petrographic microscope at 300 points per section (step 5, Fig. 3). The Gazzi-Dickinson method was used to determine composition (Gazzi, 1966; Dickinson, 1970; Ingersoll et al., 1984). The grain-size was determined by measuring the long axes of optically distinguishable grains. The median and D90 (90th percentile) grain-sizes are used for analysis as mean results were skewed by mudstone chips in some samples. Sorting was determined following Folk and Ward (1957) by measurement of the long and short axis of optically resolvable detrital grains. Detrital and authigenic clays were not distinguishable in thin-section; therefore, there is some uncertainty in inferring initial detrital clay contents. However, it is recognized that proportions of detrital matrix content in modern turbidites is variable between different bed-types (Sumner et al., 2012; Stevenson et al., 2014a; Stevenson et al., 2014b). Thinner-bedded, finer-grained distal deposits have higher detrital matrix contents compared to comparatively thicker-bedded, coarse grained deposits (Stevenson et al., 2014a; Stevenson et al., 2014b). As the clay content and trends are similar to those observed here the total clay proportion is likely to be a good indicator of original detrital clay content.

4.1 Facies

Lithofacies are summarized in Table 1 and grouped into facies associations in Table 2:

Table 1: Lithofacies observed in the study area

Facies	Lithology	Sedimentology	Thickness (m)	Interpretation	Facies cod
Mudstone	Silty claystone and clayey siltstone	Massive- to weakly-laminated.	0.01 – 2.5	Background sedimentation or deposition from a dilute flow.	LF1
Ripple laminated sandstone	Coarse-siltstone to fine-sandstone, rarely medium-sandstone.	Ripple cross-lamination, typically located in the upper parts of the bed. Climbing ripples locally observed. Commonly produces wavy bed tops.	0.02 – 0.1	Traction plus fallout from a turbulent flow (Allen, 1982; Southard, 1991; Mutti, 1992).	LF2
Planar-laminated sandstone	Very fine- to medium-sandstone.	Laminated sandstone with 0.1 m – 1mm scale alternating coarser – finer laminae. Laminae are typically parallel, rarely sub-parallel. Common coarse-tail grading. Infrequent occurrence of plant fragments and mudstone chips aligned with laminae.	0.04 – 0.5	Layer-by-layer deposition from repeated development and collapse of near-bed traction carpets (Sumner et al., 2008) and migration of low-amplitude bed-waves (Best and Bridge, 1992; Sumner et al., 2008).	LF3

Structureless sandstone	Very fine- to medium-sandstone, rare coarse-sandstone.	Typically structureless and commonly normally-graded or coarse-tail graded. Occasional mudstone chips occur, typically in fine- to coarse-sandstone beds. *Nummulites* are infrequently observed.	0.05 – 0.5	Rapid settling from a high concentration flow under hindered settling conditions (e.g. Sanders, 1965; Lowe, 1982; Mutti, 1992).	LF4
Mm-spaced laminated sandstone	Medium- to coarse-sandstone.	Laminated sandstone, laminae are 5 – 15 mm thick, parallel to sub-parallel and typically coarser-grained than surrounding sandstone. Coarser laminae are typically inversely graded.	0.1 – 0.5	Repeated collapse of traction carpets below a high-density turbidity current (e.g. Mutti, 1992; Cartigny et al., 2013), or kinetic sieving within the traction carpet (e.g. Talling et al., 2012).	LF5
Cross-bedded sandstone	Medium- to very coarse-sandstone	Centimeter- to decimeter-scale cross stratification. Foresets commonly contain clasts of mudstone or detrital material, with maximum grain-sizes of approximately 20 cm. The size of clasts reduces vertically up	0.4 – 0.65	Bed reworking by long-lived flows with relatively low depositional rates and near-bed concentrations which bypassed basin-ward (Allen and Friend, 1976; Mutti, 1992; Baas et al.,	LF6

		foresets. Transition gradually to planar laminated sandstone over 5 – 10 cm at the top.		2004; Baas et al., 2011; Talling et al., 2012).	
Conglomerate	Poorly sorted clasts of pebbles and cobbles, with infrequent boulders (max. 36 cm). Poorly sorted sandstone matrix.	Clast supported structureless deposit. Often subtle grading is present in the upper 30 cm. Clasts are usually sub- to well-rounded and include lithic fragments, quartz, limestone, mudstone and flint.	0.35 – 1.3	Deposition from a highly concentrated flow under hindered settling conditions (e.g. Walker, 1975; Lowe, 1982), or frictional freezing (Mutti, 1992).	LF7
Matrix-supported chaotic deposits	Poorly-sorted, clast-rich matrix consisting of sandstone, siltstone and mudstone.	0.2 – 25	0.2 – 25	Clast-rich, poorly-sorted, matrix supported beds are suggestive of *en-masse* deposition from laminar (debris) flows with a high yield strength (e.g. Nardin et al., 1979).	LF8

Table 2: Facies associations observed in the study area

Facies association	Description	Interpretation
FA1	An overall thinning- and fining-upwards succession 7 – 9 m thick which fill a basal incision surface. Characterized by: LF8 at the base overlain by interbedded LF2 and LF1; a sharp erosive contact to amalgamated LF7; a sharp, erosive contact to thick-bedded, amalgamated LF3, LF4 and LF6 containing abundant mudstone chips and lithic-fragments derived from LF7; a thinning- and fining-upward succession of thin-bedded, non-amalgamated LF3 and LF2.	Overall thinning- and fining-upward succession filling an incision is consistent with channel axis deposits (e.g. Mutti, 1977; Clark and Pickering, 1996; Campion et al., 2000; Sullivan et al., 2000; Beaubouef, 2004; McHargue et al., 2011; Hubbard et al., 2014; Li et al., 2016).
FA2	Thin-bedded and non-amalgamated LF3 and LF2 0.3 – 1.5 m thick. LF8 may be locally present at the base of the association. Beds are predominantly tabular and pass laterally into FA1.	Thin-bedded deposits which are adjacent to, and pass into, thicker –bedded deposits of FA1. Consistent with channel margin deposits described elsewhere (Mutti, 1977; Clark and

		Pickering, 1996; Campion et al., 2000; Eschard et al., 2003; Beaubouef, 2004; Hubbard et al., 2014; Li et al., 2016).
FA3	Commonly amalgamated packages of LF4 and LF3, with localized LF5, 4 – 6 m thick. Localized scouring on a centimeter- to meter-scale, however bed geometries are typically tabular over 10's – 100's meters.	Thick-bedded, structureless, laterally extensive beds which transition to thinner-bedded deposits on a 0.1 – 1 km scale and form packages several meters in thickness are consistent with lobe axis deposits (Prélat et al., 2009; Grundvåg et al., 2014; Marini et al., 2015).
FA4	Interbedded, infrequently amalgamated medium- and thin-bedded LF3 and LF2 packages 4 – 6 m thick. LF4 is infrequently observed. Beds typically have a sharp base and sharp top overlain by LF1. Localized, decimeter-scale scouring is observed, however beds are predominantly tabular at outcrop-scale.	Medium- and thin-bedded structured sandstones deposited predominantly from low-density turbidity currents which form meter-scale packages are consistent with lobe off-axis deposits (e.g. Prélat et al., 2009).

FA5	Thin-bedded sandstone and siltstone packages 1 – 2.5 m thick dominated by LF2 and interbedded with LF1. LF3 is infrequently observed. Amalgamation is rare. Beds typically exhibit a sharp base, and sharp top overlain by LF1. Bed geometries are tabular to wavy.	Thin-bedded, rippled, sandstones deposited by dilute low-density turbidity currents are commonly identified in lateral lobe fringe deposits (e.g. Prélat et al., 2009; Grundvåg et al., 2014; Marini et al., 2015; Kane et al., 2017; Spychala et al., 2017b). Similar facies in the Jaca Basin have previously interpreted as lobe-fringe by Mutti (1977).

5.1 Architectural element interpretations

The geometrical relationships established in the stratigraphic correlations of Figures 4 and 5, and the facies associations described in Table 2, are used to interpret the environment of deposition of the Gerbe and Broto architectural elements.

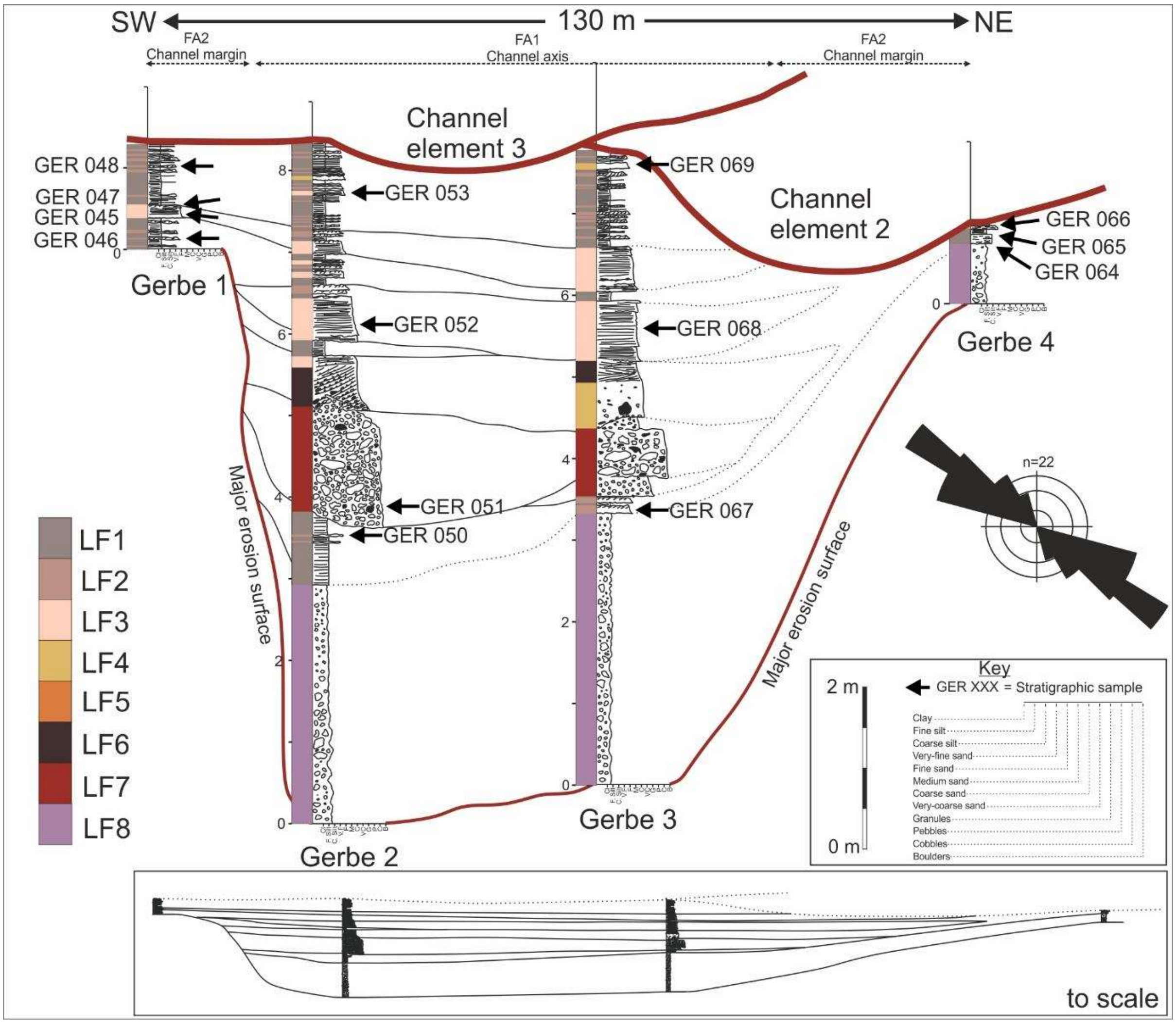

Figure 4: Architectural panel of the Gerbe channel-fill element (channel-fill element 1 of this complex). The orientation is broadly across depositional strike based on geometry and paleocurrent analysis. The channel-form is defined by a major basal erosion-surface. This is overlain by a debrite attributed to channel-excavation. The channel-fill has two main facies associations, FA1 and 2. The channel axis, FA1, is characterized by an overall thinning- and fining-upwards succession overlying LF8. The channel margins, FA2, are characterized by thin-bedded low-density turbidites.

5.2 Gerbe architectural element

The Gerbe channel-fill element is approximately 150 m wide, representing a near complete across depositional-strike transect as indicated by paleocurrent measurements (Fig. 4), and exhibits marked lateral facies changes between log localities (Fig. 4). The measured sections at localities (localities refer to measured sections herein) Gerbe 2 and Gerbe 3 are 8.5 m and 7.9 m thick respectively and are characterized by FA1 (Figs. 4, 6B and D). The Gerbe 1 and Gerbe 4 localities are 1.4 m and 1.1 m, respectively, and are characterized by FA2 (Figs. 4, 6A).

5.3 Broto architectural element

The Broto lobe (Lobe 1 of Bell et al., *in press;* Fig. 5), has a comparatively tabular geometry and is approximately 16 km in length and more than 0.9 km wide (Fig. 5A, B). The element exhibits more-gradual lateral facies changes compared to the Gerbe channel-fill element (Fig. 5A, B). The base and top of the architectural element are marked by a debrite (Figs. 5D, 6E) and a laterally persistent thin-bedded package that can be correlated on a kilometer-scale between outcrops (Fig. 6G), respectively. The Fanlo 1, Fanlo 2 and Fanlo Track localities predominantly consist of FA3, and are interpreted as lobe axis deposits (Fig. 5, 6E; e.g. Prélat et al., 2009). The A Lecina, Oto and Linás de Broto localities are characterized by FA4 and are interpreted as lobe off-axis (Fig. 6F; e.g. Prélat et al., 2009). The Yésero locality consists of FA5 and is interpreted as the lobe fringe (Fig. 6H; e.g. Prélat et al., 2009). The observed facies changes and geometries are consistent with lobes observed elsewhere (e.g. Prélat et al., 2009; Grundvåg et al., 2014; Marini et al., 2015; Kane et al., 2017; Spychala et al., 2017a), and have previously been interpreted as lobes within the Jaca Basin (Mutti, 1977; Mutti, 1992; Bell et al., *in press*).

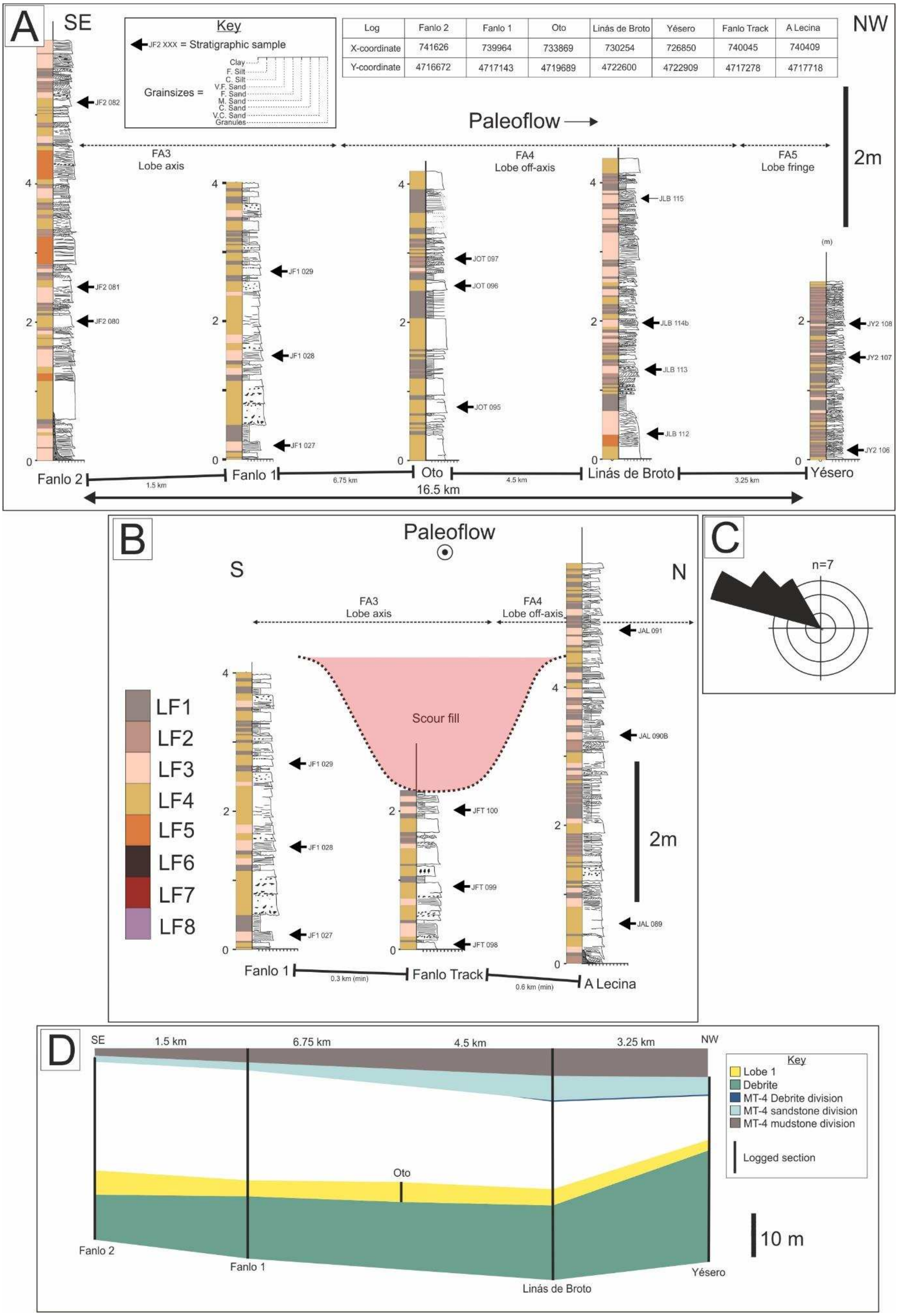
A
SE
NW
Key
JF2 XXX = Stratigraphic sample
Grainsizes =
Clay
F. Silt
C. Silt
V.F. Sand
F. Sand
M. Sand
C. Sand
V.C. Sand
Granules
Log | Fanlo 2 | Fanlo 1 | Oto | Linás de Broto | Yésero | Fanlo Track | A Lecina
X-coordinate | 741626 | 739964 | 733869 | 730254 | 726850 | 740045 | 740409
Y-coordinate | 4716672 | 4717143 | 4719689 | 4722600 | 4722909 | 4717278 | 4717718
Paleoflow
2m
FA3
Lobe axis
FA4
Lobe off-axis
FA5
Lobe fringe
JF2 082
JF2 081
JF2 080
JF1 029
JF1 028
JF1 027
JOT 097
JOT 096
JOT 095
JLB 115
JLB 114b
JLB 113
JLB 112
JY2 108
JY2 107
JY2 106
(m)
Fanlo 2
Fanlo 1
Oto
Linás de Broto
Yésero
1.5 km
6.75 km
4.5 km
3.25 km
16.5 km
B
Paleoflow
S
N
FA3
Lobe axis
FA4
Lobe off-axis
Scour fill
JF1 029
JF1 028
JF1 027
JFT 100
JFT 099
JFT 098
JAL 091
JAL 090B
JAL 089
2m
LF1
LF2
LF3
LF4
LF5
LF6
LF7
LF8
Fanlo 1
Fanlo Track
A Lecina
0.3 km (min)
0.6 km (min)
C
n=7
D
SE
NW
1.5 km
6.75 km
4.5 km
3.25 km
Oto
Fanlo 2
Fanlo 1
Linás de Broto
Yésero
Key
Lobe 1
Debrite
MT-4 Debrite division
MT-4 sandstone division
MT-4 mudstone division
Logged section
10 m

Figure 5: Architectural panels of Lobe 1 of the Upper Broto system: A) Depositional-dip correlation of Lobe 1, from lobe axis at Fanlo 2 to frontal lobe fringe at Yésero; B) Depositional-strike architecture of Lobe 1, from lobe axis at Fanlo 1 and Fanlo Track to lobe off-axis at A Lecina; C) Paleocurrents measured in Lobe 1 suggest flow to the northwest, consistent with other studies within the basin (e.g. Mutti 1977, 1984, Remacha et al., 2005, Bell et al., *in press*); D) Stratigraphic context of down depositonal-dip correlation panel showing Lobe 1 in relation to key marker beds (modified from Bell et al., *in press.).*

Gradual facies changes over 100's – 1000's meters in Lobe 1 contrast to distal deposits of the Upper Broto System (i.e. the basin plain, *sensu* Remacha et al., 2005). Northwest of Jaca (Fig. 1A) basin-plain deposits exhibit more tabular cross-sectional geometries, with less lateral variability, and do not form lobes (Remacha and Fernández, 2003; Remacha et al., 2005; Bell et al., *in press*). An idealized basin-plain bed comprizes: a clean basal sandstone, overlain by a clast-rich, poorly-sorted division, followed by a thick mudstone cap with an upper-carbonate-rich division (Remacha and Fernández, 2003; Remacha et al., 2005; Bell et al., *in press*). Bases of basal clean sandstone divisions have flute and tool marks suggesting flow to the west/northwest. Upper surfaces of some sandstone beds have ripple cross laminations suggesting paleoflow to the north, interpreted to form due to flow deflection from the southern, carbonate slope (Remacha and Fernández, 2003; Remacha et al., 2005; Bell et al., *in press*). Poorly sorted divisions are interpreted to form either through: repeated deposition and liquefaction of lamina from bores within deflected turbulent flows (Remacha and Fernndez, 2003, Remacha et al., 2005); or from turbulent flows which collapsed to form predominantly laminar flows during flow deflection (Bell et al., *in press*).

6.1 Results

Architectural and textural data were collected for both the channel-fill element and lobe. Textural properties are split into facies associations for each architectural element to enable comparison of architectural and textural properties, and consequent depositional reservoir quality in different sub-environments within deep-water systems.

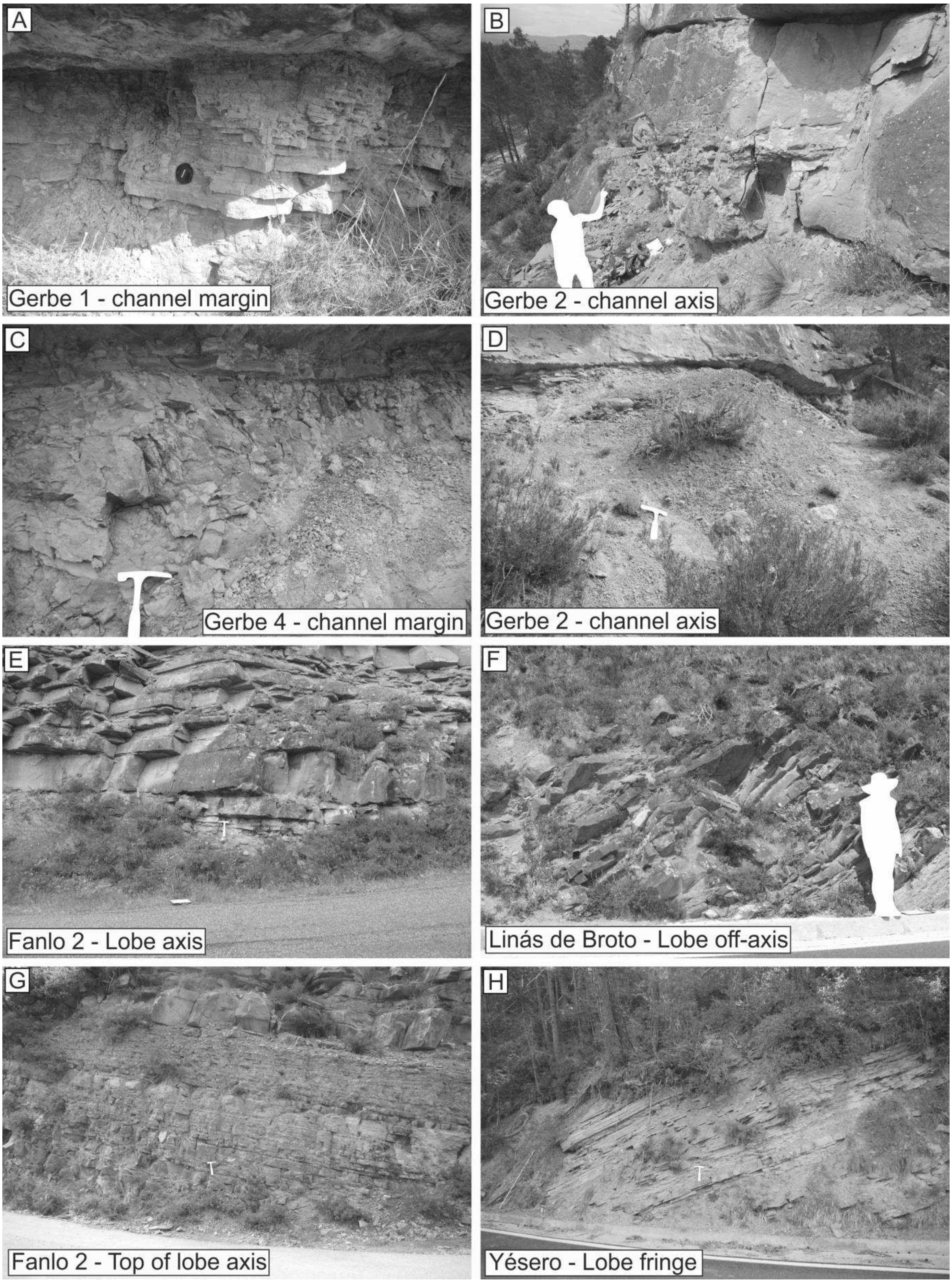
A
Gerbe 1 - channel margin
B
Gerbe 2 - channel axis
C
Gerbe 4 - channel margin
D
Gerbe 2 - channel axis
E
Fanlo 2 - Lobe axis
F
Linás de Broto - Lobe off-axis
G
Fanlo 2 - Top of lobe axis
H
Yésero - Lobe fringe

Figure 6: A) Channel-margin facies: structured sandstones and siltstones deposited from low-density turbidity currents; B) Channel-axis facies, from the base: pebbly mudstone, conglomerate and cross-bedded sandstone. The cross-bedded sandstone has an erosional base and overlies the conglomerate, with evidence for substrate entrainment; C) Channel-margin siltstones overlying pebbly-mudstone; D) Channel-axis pebbly-mudstone erosively overlain by thick-bedded sandstone; E) Amalgamated, thick-bedded lobe axis sandstones. Onlap of beds onto the underlying debrite is observed to the right of the hammer (length 28 cm); F) Medium-bedded lobe off-axis; G) Thin-bedded package overlying Lobe 1 at Fanlo 2. Top of Lobe 1 is at the base of the hammer; H) Thin-bedded lobe-fringe sandstones and siltstones at Yésero.

6.2 Composition

6.2.1 Siliciclastic detrital grains

Non-carbonate detrital grains consist of: monocrystalline quartz (6% – 23.7%), polycrystalline quartz (up to 4.3%), plagioclase feldspar (up to 14.3%), K-feldspar (trace), sedimentary rock fragments (up to 3.3%), metamorphic rock fragments (up to 3.7%), igneous rock fragments (up to 3.7%), muscovite (up to 1.3%) and trace minerals.

6.2.2 Carbonate detrital grains

Carbonate grains are common and can make up the largest group of detrital grains within a sample (6.3 – 27.3%). Carbonate grains consist of dolostone, sparitic limestone, micritic limestone, peloids, aggregate grains and fossils. Fossils identified in thin section include foraminifera (benthic and planktonic), gastropods, algae and echinoderm fragments.

6.2.3 Authigenic minerals

Calcite is the dominant authigenic mineral within the samples (19.7% – 38.3% of grains counted), present as both pore-filling cement and replacement of detrital grains. Minor amounts of authigenic quartz (typically <5%, but locally up to 12%) are identified, typically as overgrowths or pore-filling cement. Traces of authigenic plagioclase and oxide minerals are present, typically <1%.

6.2.4 Matrix minerals

Matrix-mineralogy is not optically resolvable. However, where present, matrix is typically identified between or coating larger grains. Pseudomatrix consisting of ductile grains (typically mudstone or micritic limestone) is commonly observed within samples.

6.2.5 Classification

A standard ternary plot of quartz-feldspar-lithic fragments indicates that most samples are categorized as sublitharenites (Fig. 7; see also: Das Gupta and Pickering, 2008; Caja et al., 2010). Linked channel and lobe deposits are shown to exhibit compositional differences (e.g. Stalder et al., 2017). Here, Gerbe samples are more quartz-rich, with some classified as quartz arenites, whereas Broto samples are more feldspar-rich (Fig. 7). This study primarily concerns textural properties and trends, and so composition is not discussed in depth. Compositional evolution, classification and provenance within the Hecho Group are reported in Fontana et al. (1989), Zuffa et al. (1995), Das Gupta and Pickering, (2008), and Caja et al. (2010).

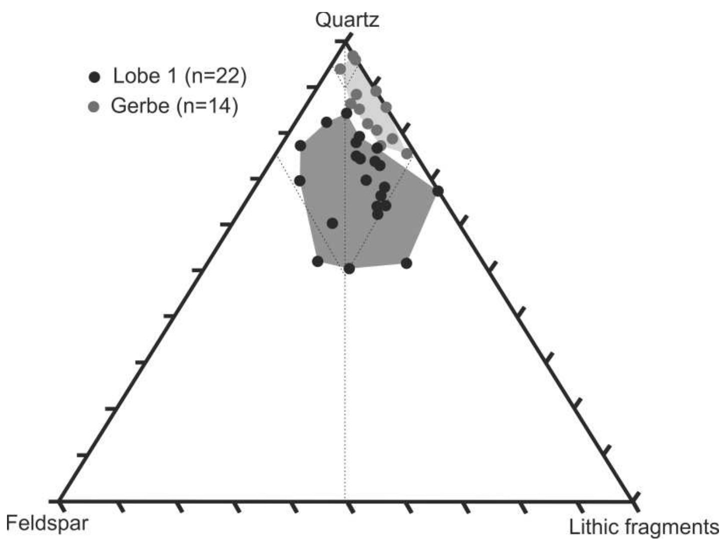

Figure 7: QFL (Quartz, Feldspar, Lithic fragments) plots from the 36 point-counted thin-sections, assigned to each study area. Most samples are classified as sub-litharenites. However, the Gerbe samples are typically more quartz-rich and feldspar-poor compared to Lobe 1 samples. Ternary plot after Pettijohn et al. (1972).

Table 3: Architectural and textural properties at each logged section.

Basin	Locality	Net sandstone thickness (m)	Sandstone %	%Amalgamated	Median grain-size (mm)	D90 (mm)	Sorting (F&W)	Mean matrix%	Mean authigenic %
Aínsa	Gerbe 1	0.425	31.3	14.286	0.090	0.127	0.225	25.675	31.900
Aínsa	Gerbe 2	3.360	39.3	15.385	0.098	0.161	0.181	19.633	39.467
Aínsa	Gerbe 3	3.680	46.5	39.394	0.109	0.155	0.205	14.433	47.667
Aínsa	Gerbe 4	0.040	3.6	0.000	0.041	0.053	0.245	34.333	36.900
Jaca	Fanlo 2	5.510	90.0	78.378	0.150	0.212	0.204	7.556	36.111
Jaca	Fanlo 1	3.100	77.1	67.742	0.175	0.285	0.134	8.556	31.222
Jaca	Oto	2.895	68.9	38.095	0.096	0.141	0.188	15.778	35.889
Jaca	Linás de Broto	3.220	73.7	34.091	0.166	0.316	0.199	15.833	33.417
Jaca	Yésero 2	1.385	54.1	3.636	0.056	0.079	0.174	29.000	32.444
Jaca	A Lecina	3.945	67.3	28.571	0.169	0.235	0.208	15.444	36.333

Jaca	Fanlo Track	1.750	76.1	62.500	0.250	0.369	0.173	8.433	37.900

Table 4: Architectural and textural properties of facies associations

Basin	**Sub-environment**	**Avg. sandstone thickness (m)**	**Avg. sandstone %**	**Avg. %amalgamated**	**Avg. median grain-size (mm)**	**Avg. D90 (mm)**	**Avg. sorting (F&W)**	**Avg. mean matrix%**	**Avg. mean authigenic %**
Aínsa	Channel-axis	3.520	42.9	27.389	0.103	0.158	0.193	17.033	43.567
Aínsa	Channel-margin	0.233	17.4	7.143	0.065	0.090	0.235	30.004	34.400
Jaca	Lobe axis	3.453	81.1	69.540	0.192	0.289	0.170	8.181	35.078
Jaca	Lobe off-axis	3.353	70.0	33.586	0.143	0.230	0.198	15.685	35.213
Jaca	Lobe fringe	1.385	54.1	3.636	0.056	0.079	0.174	29.000	32.444

6.3 Gerbe Channel-fill element

6.3.1 Architectural- and bed-scale data

The thickness of the Gerbe channel-fill element increases from Gerbe 1 and 4 to Gerbe 2 and 3 respectively (Fig. 4). The proportion of amalgamated sandstone beds is similar between the channel-margin at Gerbe 1 and channel-axis at Gerbe 2; however, the amalgamation ratio is higher at Gerbe 3, and lower at Gerbe 4 (Figs. 8B; Tables 3, 4). Sandstone-percentage is similar in the channel-axis and channel-margins due to the debrite located in the channel-axis, however the total thickness of sandstone is greater in the channel-axis (Fig. 8B; Table 4).

6.3.2 Lateral variation in texture

Grain-size varies within the channel-fill sandstones (Figs. 8A, 9; Table 3). The median grain-size slightly increases from the western channel-margin Gerbe 1, into the channel-axis deposits of Gerbe 2 and 3 (440 µm/km; Figs. 8A, 10; Table 3). Median grain-size then decreases to the eastern channel-margin at Gerbe 4 (1130 µm/km; Fig. 8A; Table 3). The D90 (90^{th} percentile of grain-size) shows a similar trend, increasing from Gerbe 1 to Gerbe 2 and 3 (1700 µm/km; Figs. 8A, 10; Table 3). The D90 at Gerbe 4 is finer than in other positions (Fig. 8A; Table 3). The optically-resolvable detrital grains of the channel-margin deposits are better sorted compared to the channel-axis deposits (Fig. 8A Table 3). The authigenic mineral content increases from the channel-margins into the channel-axis positions (Fig. 8B; Table 4). Channel-margin deposits at Gerbe 1 and 4 have higher matrix content compared to channel-axis deposits at Gerbe 2 and 3 (Fig. 8B; Tables 3, 4). Matrix content increases from Gerbe 2 to 1, and Gerbe 3 to 4 at a rate of 310 %/km and 340 %/km respectively (Fig. 10).

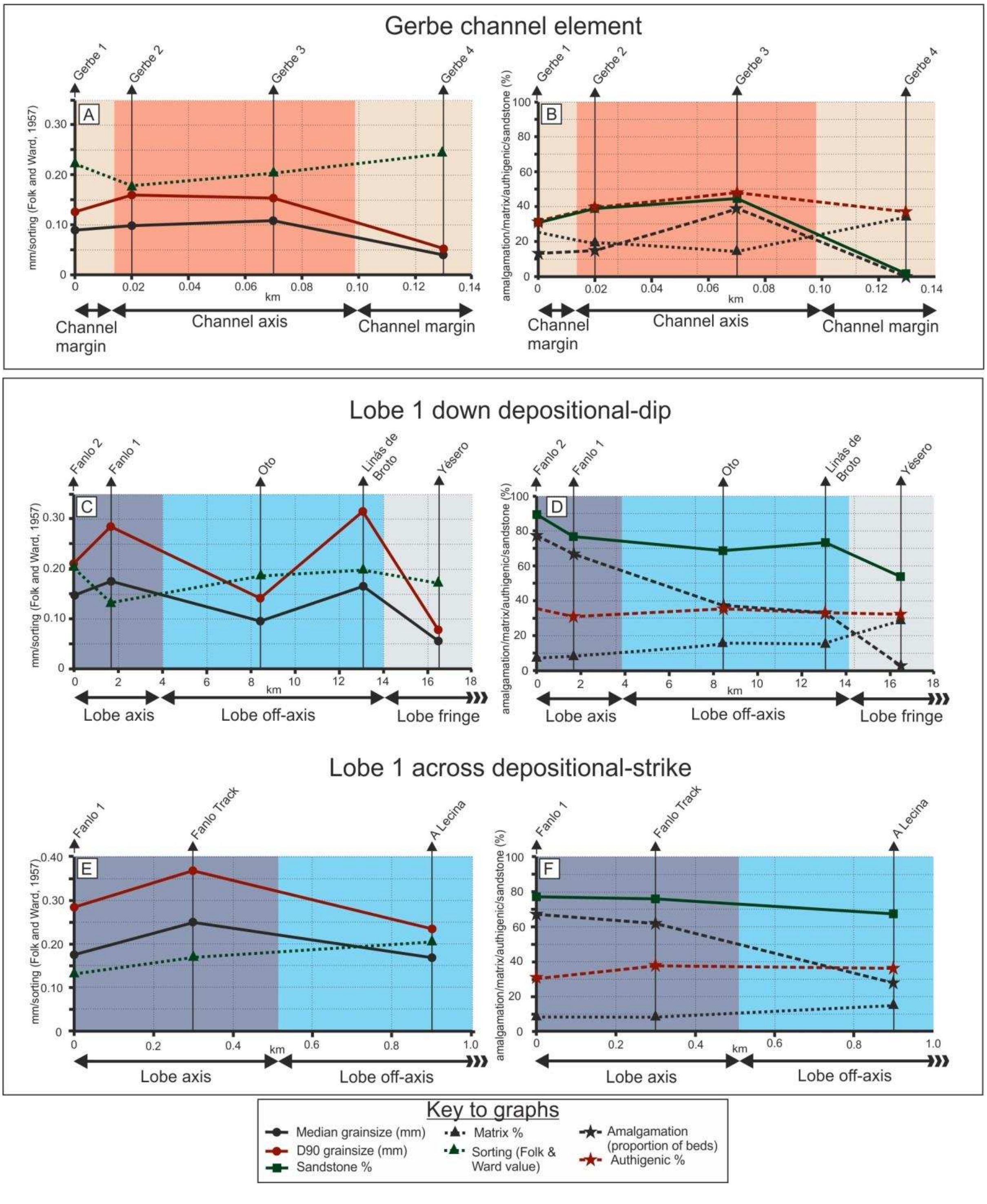

Figure 8: Spatial variation in textural and architectural properties within Lobe 1 and the Gerbe channel-fill element.

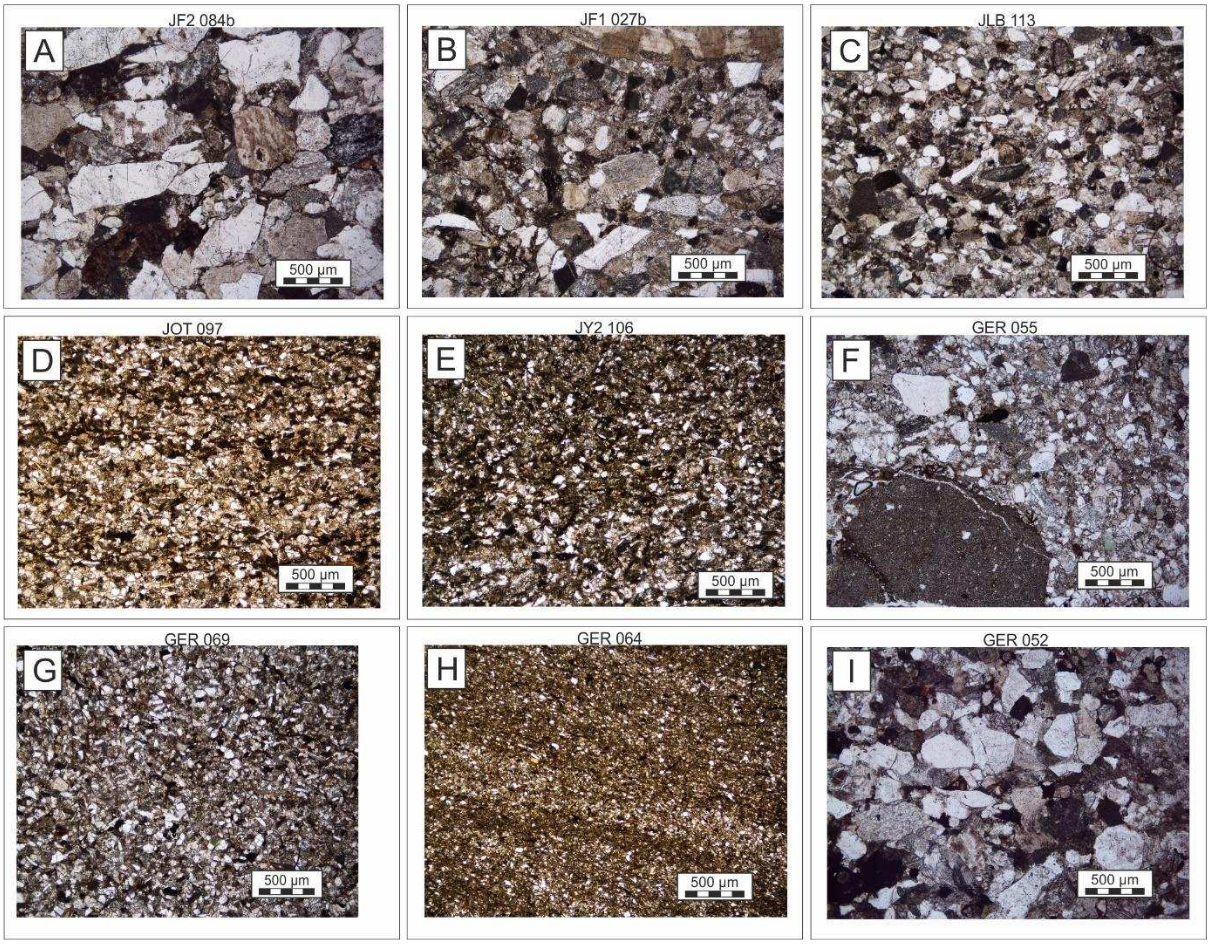

Figure 9: Example grain-scale textures of lithofacies: A) High-density turbidite from lobe axis setting; B) High-density turbidite from lobe axis setting. A foram test is present at the top of the sample; C) Low-density turbidite from lobe off-axis setting; D) Low-density turbidite from lobe off-axis setting; E) Low-density turbidite from lobe fringe setting; F) Channel-axis conglomerate, with large fine-grained dolostone clast; G) Low-density turbidite from channel-axis setting; H) Ripple cross-laminated low-density turbidite from channel-margin setting; I) High-density turbidite from channel-axis setting.

6.3.3 Vertical textural variation

Textural properties also vary vertically within the Gerbe channel-fill element (Figs. 9, 11). Overlying the basal debrite, channel-axis deposits show an increase in grain-size (both median and

D90) from thin-beds (>4 m on Figs. 11A, B) into the thicker-bedded, amalgamated conglomerate and sandstone (2 – 4 m on Figs. 11A, B). There is a fining upward profile into the thinner-bedded deposits in the upper 2 m (Figs. 11A, B). Channel-margin positions show a general fining upward trend in both median and D90 grain-sizes (Figs. 11A, B). Sorting improves upwards in both channel-axis and channel-margin deposits (Fig. 11B), a decrease in sorting at 5.2 m at Gerbe 2 is observed within the conglomerate sample. There is no clear trend to vertical variation in authigenic mineral content, however an upward decrease is observed at Gerbe 1 (Fig. 11D). There is a general upward increase in matrix content at all positions (Fig. 11E). At channel-axis positions matrix content decreases from the lower thin-bedded deposits into the thick-bedded amalgamated sandstones located between 2 and 4 m (Fig. 11E). Matrix content then shows a general increase upwards into the overlying thinner-bedded deposits (Fig. 11E).

6.4 Lobe 1

6.4.1 Architectural data

The thickness of Lobe 1 decreases from 6.1 m in the most proximal position (Fanlo 2) to 2.6 m in the most distal position (Yésero; Fig. 5A). Thickness increases across depositional strike from Fanlo 1 to the lobe off-axis position of A Lecina (Fig. 5B). The proportion of amalgamated beds decreases down-dip from Fanlo 2 to Yésero (4.5%/km; Figs. 8D, 10; Table 3), and across strike from Fanlo 1 to A Lecina (Fig. 8F; Table 3). The degree of amalgamation higher in lobe axis deposits compared to lobe off-axis and lobe fringe deposits (Fig. 8D; Table 4). Sandstone-percentage decreases from Fanlo 2 to Yésero (2.8%/km; Figs. 8D, 10; Table 3). Across-strike, the sandstone-percentage decrease from Fanlo 1 to A Lecina is l

ess pronounced (Fig. 8F; Table 3). Lobe axis deposits exhibit a higher sandstone proportion than lobe off-axis and lobe fringe deposits (Table 4).

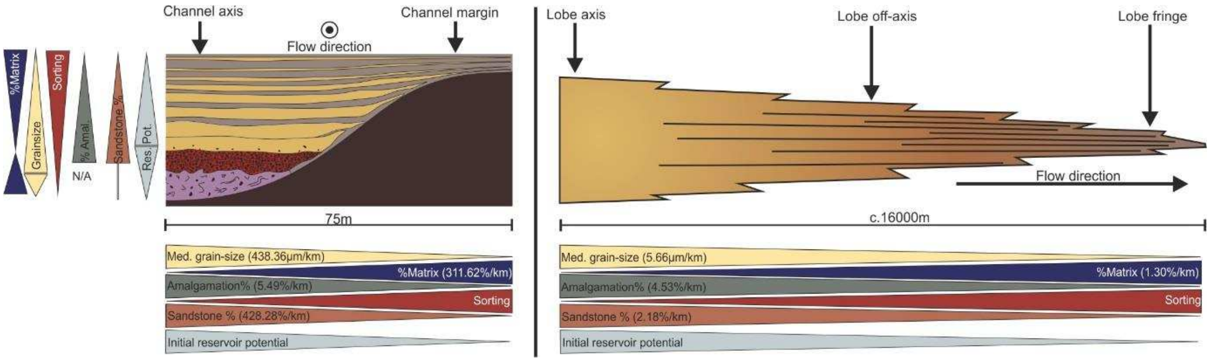

Figure 10: Schematic illustration of the spatial variation in architectural and textural properties within deep-water channel-fill elements and lobes. Within the lobe, textural and architectural properties vary most-strongly laterally. The channel-fill element shows strong trends in textural and architectural properties both laterally and vertically. The inferred reservoir quality decreases from lobe axis to lobe fringe, and from channel-axis to channel-margin. Reservoir quality also decreases vertically within the Gerbe channel-fill element, if the basal non-reservoir debrite is not included. The lateral gradient of change in properties is typically around two orders of magnitude greater within the channel-fill element compared to the lobe.

6.4.2 Textural data

Textural properties vary spatially within Lobe 1 (Figs. 8C and E, 9; Table 3). Overall, median grain-sizes decrease down-dip from Fanlo 2 to Yésero (6 µm/km; Figs. 8C, 10; Table 3). Across strike, median grain-size decreases from Fanlo 1 and Fanlo Track, to A Lecina (Fig. 8E; Table 3). The D90 decreases down-dip from Fanlo 2 to Yesero (5 µm/km; Figs. 8A, 10; Table 3). D90 increases northwards, across strike from Fanlo 1 to Fanlo Track, but is lower at A Lecina (Fig. 8E; Table 3). In both measurements of grain-size, there is a down-dip increase from Oto to Linás de Broto (Fig. 8C; Table 3). Sorting is relatively consistent throughout Lobe 1, with most samples categorized as moderately or moderately-well sorted (Figs. 8C, E; Table 3; *sensu* Folk and Ward, 1957).

The proportion of authigenic minerals shows little variation across Lobe 1 (Fig 8D, F; Table 3). Positions with the highest authigenic mineral contents are in proximal areas (Fanlo 2, Fanlo Track, A Lecina, and Oto; Figs. 8D, F; Table 3); however, Fanlo 1 has the lowest authigenic mineral content (Figs. 8D, F; Table 3). The proportion of matrix increases down-dip from Fanlo 2 to Yésero (Fig. 8D; Table 3). Matrix content also increases across-strike from Fanlo 1 to A Lecina (Fig. 8F; Table 3).

Lobe axis deposits exhibit the coarsest median grain-sizes compared to lobe off-axis and lobe fringe deposits (Figs. 8C and E, 9; Table 3); and coarser D90 grain-sizes compared to lobe off-axis deposits (Figs. 8C and E, 12B and C; Table 3). The lobe fringe has a much lower D90 (Figs. 8C, 12B and C; Table 3). Sorting increases from lobe axis deposits into lobe off-axis deposits, and decreases from lobe off-axis deposits into the lobe fringe deposits (Figs. 8C and E, and 12C and D; Table 4).

Lobe axis and lobe off-axis deposits exhibit marginally higher contents of authigenic minerals than the lobe fringe deposits (Fig. 12A; Table 4). Lobe axis deposits exhibit the lowest matrix contents, lobe off-axis deposits have medial matrix contents, and the lobe fringe deposits have the highest matrix content (Figs. 8D and F, 12A, B and D; Table 4). The rate of change is different between the lobe axis and lobe off-axis, and lobe off-axis and lobe fringe. Matrix content increases at 0.6 %/km between Fanlo 2 and Linás de Broto, compared to 3.8 %/km between Linás de Broto and Yesero (Lobe overall increase is 1.3 %/km; Figs. 8D, 10).

6.5 Comparison of textural properties

Scatter plots of textural properties suggest channel-margin and channel-axis deposits have different textural characteristics (Fig. 12). Higher proportions of matrix correspond to lower proportions of authigenic minerals in the Gerbe samples (Fig. 12A). Increased matrix content also corresponds to finer grain-sizes and better sorting of detrital grains in the samples (Fig. 12B, C). Decreases in grain-size are associated with improved sorting of detrital grains, and increased matrix content (Fig. 12B, D). Channel-margin deposits (Gerbe 1 and 4) have fine grain-sizes, high proportions of matrix, low proportions of authigenic minerals and better sorting (Figs. 8A and B, 12; Table 4). Comparatively, channel-axis deposits exhibit coarser grain-sizes, lower proportions of matrix, higher proportions of authigenic minerals, and are more poorly sorted (Figs. 8A and B, 12; Table 4).

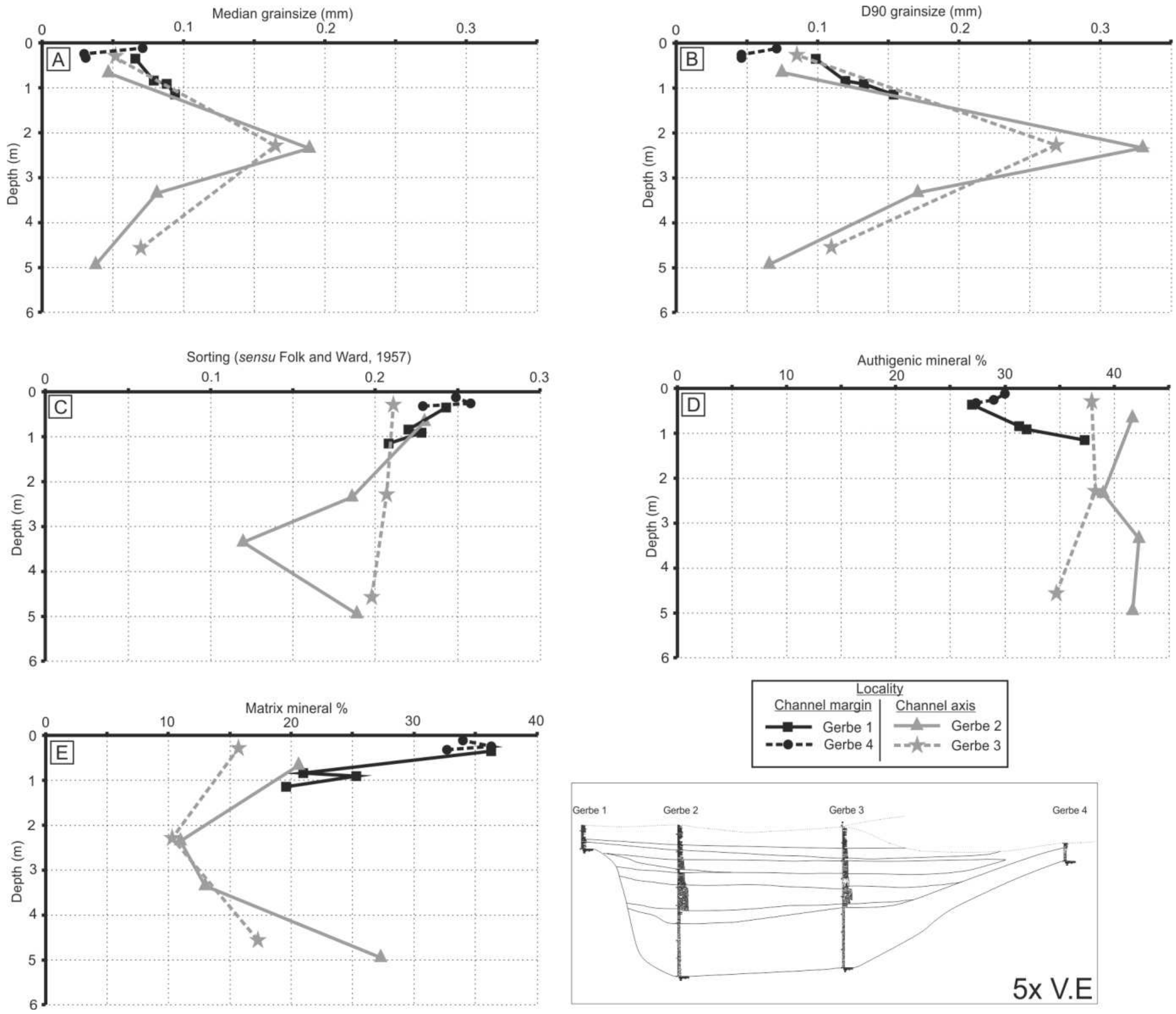

Figure 11: Vertical variation in textural properties at each Gerbe logged section. The top of each section is used as a datum. Grain-size typically decreases upwards within the channel fill (A and B). Within the channel-axis there is an apparent initial increase in grain-size. This is attributed to the upward transition from a package of thin-beds, interpreted as the deposits of the dilute tails of larger flows which bypassed the locality, to the main aggradational-fill of the channel. Sorting increases upwards within the channel-fill (C). The most poorly-sorted sample (~3.2 m Gerbe 2) is a conglomerate (LF6). Vertical changes in authigenic content are not strongly developed (D). The proportion of matrix increases upwards within the

channel-fill (E). The initial decrease in the channel-axis represents the transition from the initial bypass-phase to the main aggradational-phase of sand deposition.

Lobe 1 exhibits a similar separation of textural properties. Increasing matrix content correlates with decreasing grain-size and better sorting (Fig. 12A, B, D). Matrix and authigenic mineral contents do not exhibit a strong relationship (Fig. 12A). Samples with coarser grain-sizes also exhibit poorer sorting compared to samples with finer grain-sizes (Fig. 12C). Separate groupings of lobe axis, lobe off-axis and lobe fringe samples suggests the sub-environments have distinct textural properties (Fig. 12) although this is likely to form part of a continuum.

Comparison of channel-fill element and lobe sub-environment deposits shows similarities between the different architectural elements (Fig. 12). Positions dominated by thinner-bedded deposits (channel-margin and lobe fringe) have finer grain-sizes, higher matrix content, are better sorted and have marginally lower authigenic mineral content compared to positions with thicker-bedded channel-axis and lobe axis deposits (Fig. 12; Table 4). Channel-axis and lobe off-axis deposits show the greatest range in textural properties (Fig. 12; Table 4), especially in grain-size and matrix content (Fig. 12; Table 4).

The rate of change of textural properties is typically around two orders of magnitude more abrupt in the channel-fill element (channel axis to channel margin) in comparison to the lobe (Fig. 10).

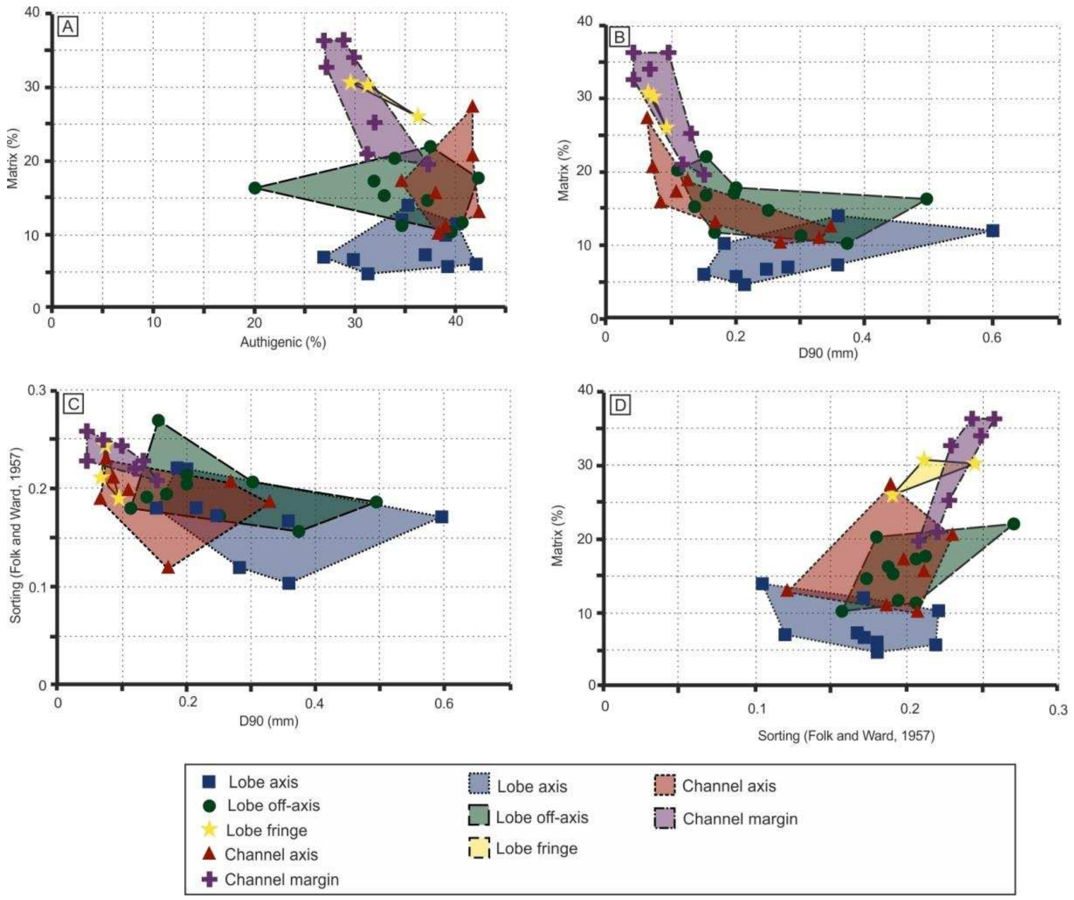

Figure 12: Variation of textural properties within channel and lobe sub-environments. Samples are grouped by sub-environment interpretations. Channel margin and lobe fringe samples show overlap and consistently have comparatively finer grain-sizes and higher matrix contents. Channel axis and lobe off-axis samples overlap and exhibit a mix of grain-sizes and matrix contents. The lobe axis samples typically plot in a discrete area due to coarser grain-sizes and lower matrix contents.

7.1 Discussion

7.2 Spatial variation in depositional reservoir quality

The distribution of textural properties (grain-size, sorting and matrix content) within architectural elements is a first-order control on the initial depositional porosity and permeability of sandstones (e.g. Fraser, 1935; Beard and Weyl, 1973; Hirst et al., 2002; Lien et al., 2006; Njoku and Pirmez, 2011; Kilhams et al., 2012; Marchand et al., 2015; Porten et al., 2016; Southern et al., 2017) and provides insight into the depositional reservoir quality within the study area. The effects of post-depositional modification are not discussed unless explicitly stated.

7.2.1 Gerbe channel-fill element

Textural properties vary both laterally and vertically within the Gerbe channel-fill element (Figs. 8, 9, 10, 11, 12). Grain-size increases and matrix content decreases from channel-margins to channel-axis (Figs. 8, 10, 11, 12). In unconsolidated sand, as grain-size increases pore throats become larger and permeability increases (e.g. Beard and Weyl, 1973). However, changes in grain-size do not affect porosity within deposits with the same degree of sorting (Beard and Weyl, 1973). This suggests that initial permeability would have been higher in channel-axis deposits. Grain-size also decreases stratigraphically within the Gerbe channel-fill element (Fig. 11A, B), suggesting initial permeability decreased upwards. Sorting is better in the channel-margins, and also increases vertically within the channel-fill (Figs. 8, 11, 12). Well-sorted deposits exhibit higher porosity and permeability in unconsolidated sand as smaller grains fill intergranular space and block pore throats in poorly-sorted deposits (Beard and Weyl, 1973). However, the overall effect of sorting on reservoir quality is currently inconclusive, as grain-size and clay content often mask its effect (Lien et al., 2006; Porten et al., 2016; *c.f.* Njoku and Pirmez, 2011). This is likely an artefact of traditional point counting methods, which calculate sorting data from optically resolvable grains (i.e. not clays). Therefore, channel margin and lobe fringe deposits in which hydraulic fractionation resulted in well-sorted detrital grains, but with a high-matrix content, appear well-sorted. In contrast, the deposits of relatively poorly-stratified, high-density flows are likely to have poorer-sorting of detrital grains, but low-matrix contents. High matrix content in channel margin positions (Figs. 8, 10, 11, 12) likely reduced both initial porosity and permeability as detrital clay can impact reservoir quality by blocking pore throats and reducing permeability (Fraser, 1935; Hirst et al., 2002; Lien et al., 2006; Porten et al., 2016). Authigenic mineral content is highest in the channel axis (Fig. 8B), suggesting a higher initial porosity, and that fluid flow was greater in these deposits prior to mesodiagenesis, suggesting higher initial permeabilities.

Both sandstone-percentage and the proportion of amalgamated beds decrease from channel-margin to channel-axis (Fig. 8B, 10). Therefore, channel-axis deposits exhibit better depositional reservoir quality at both grain-scale (porosity and permeability) and architectural element scale (sandstone-percentage and amalgamation) compared to channel-margin deposits (Fig. 10).

Whilst the depositional reservoir quality of channel-axis sandstones is better compared to the channel margin, the channel-axis in this case contains a thick mudstone-rich debrite. This debrite would have poor reservoir properties (e.g. Hirst et al., 2002), and reduce the overall vertical permeability and depositional reservoir quality of the channel axis. However, incision of channel-fill element one by channel-fill elements two and three improves vertical connectivity of channel-axis sandstones in the channel-complex axis (Fig. 4).

7.2.2 Process controls on depositional reservoir quality distribution

Cycles of channel initiation, incision, and filling record a complicated waxing-waning history of flow energy, and associated sediment bypass and aggradation (e.g. Mutti and Normark, 1987; Mutti, 1992; Clark and Pickering, 1996; McHargue et al., 2011; Hubbard et al., 2014; Stevenson et al., 2015). The basal channel surface is interpreted to be excavated by a debris flow, or flows (e.g. Dakin et al., 2013), which deposited the debrite. The debrite is erosively overlain by siltstone and discontinuous thin sandstone beds, interpreted to represent a bypass-dominated channel-base-drape (e.g. Hubbard et al., 2014; Stevenson et al., 2015). Silt-prone drapes act as barriers to flow, but notable detrimental effects are only observed with cross-sectional drape coverages in excess of 60% (e.g. Barton et al., 2010). Subsequent channel-axis aggradation is dominated by amalgamated high-density turbidites (Figs. 4, 13), resulting in high sandstone-percentage and connectivity. The fill progressively thins and fines upward into thin-bedded low-density turbidites (Figs. 4, 13). Channel-margin deposits are characterized almost exclusively by low-density turbidites (Figs. 4, 13). Topography steers high-density turbidity currents more-strongly than low-density turbidity currents (e.g. Al Ja'aidi et al., 2004), and so focussing of high-density turbidity currents within the thalweg concentrates the best reservoir properties in the channel-axis (Figs. 10, 13). Low-density flows, or low-density parts of stratified flows, are able to surmount topography, depositing low-density turbidites contemporaneously on the channel-margin (Fig. 13A, B; e.g. Hiscott et al., 1997). In later stages of channel aggradation, the channel-cut is partly-to-fully filled due to system back-stepping through relative sea-level rise, or other mechanisms, reducing flow-volume and sediment supply to the channel-fill (e.g. Mutti and Normark, 1987; Clark and Pickering, 1996; Campion et al., 2000; Gardner and Borer, 2000; McHargue et al., 2011; Di Celma et al., 2014; Hubbard et al., 2014; Hodgson et al., 2016). Reduction of sediment supply and smaller flow-volume means later flows reaching a given location are finer-grained, more-dilute and have poorer reservoir potential compared to earlier aggradational deposits.

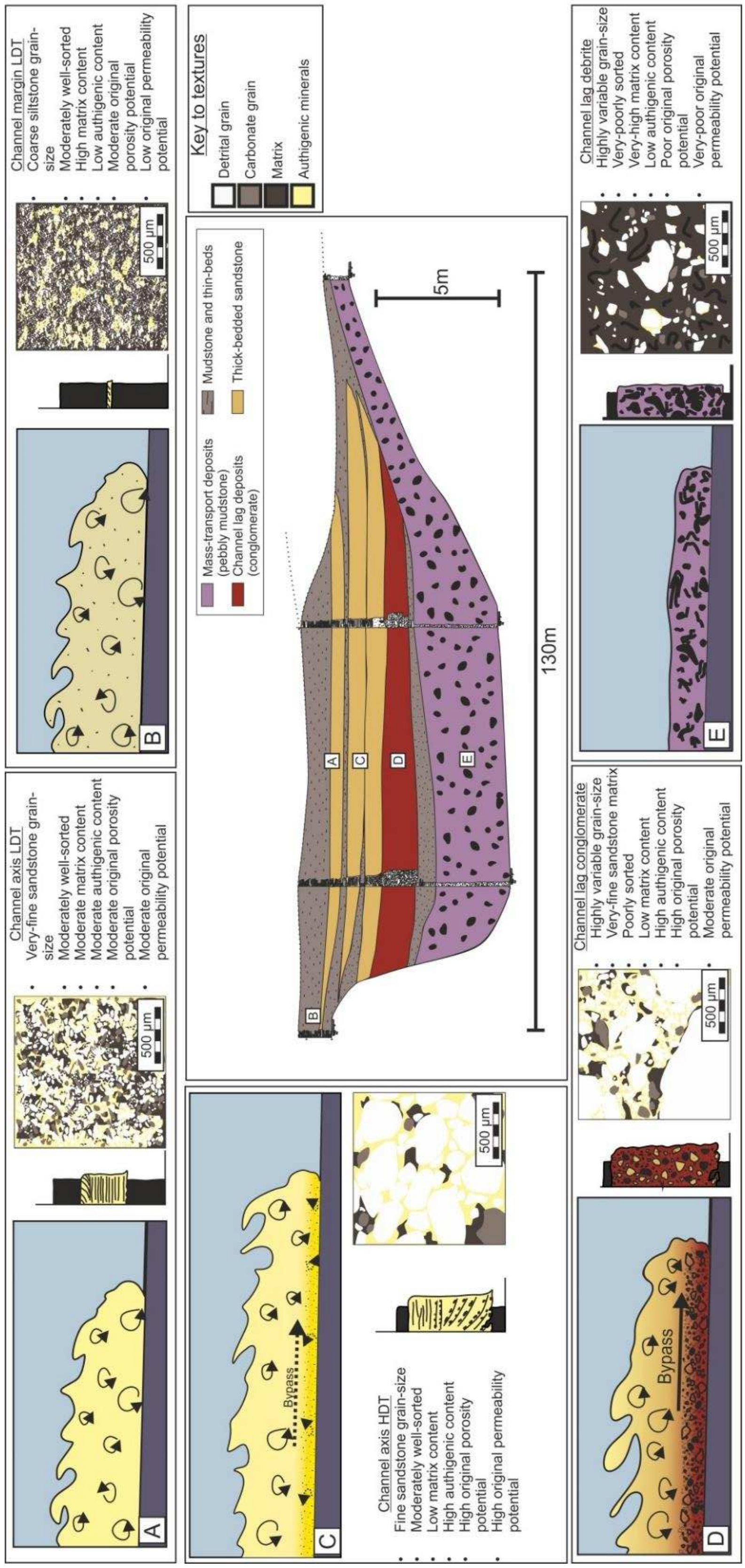

Figure 13: Flow process controls on channel-fill reservoir potential. The lower channel-axis is filled by debrites (E), which are poorly-sorted, mudstone-rich and low reservoir potential. Conglomerate (D),

representative of a high-concentration, strongly bypassing flow. Reservoir potential in initial channel-axis deposits is high due to amalgamation of high-density turbidites (C and D). Decreases in amalgamation and grain-size, and increases in matrix content vertically and laterally reduce depositional reservoir quality. The upper channel-fill element fill axis (A) and channel-margins (B) are dominated by non-amalgamated low-density turbidites and have poorer grain-scale reservoir potential.

7.2.3 Lobe 1

Within Lobe 1, the decrease in grain-size from lobe axis to lobe fringe positions (Figs. 8C, 9, 10 12) suggests that initial permeability decreased away from the lobe axis. The proportion of matrix increases from lobe axis to lobe fringe (Figs. 8C, 12; see also: Hirst et al., 2002; Marchand et al., 2015; Kane et al., 2017; Fildani et al., 2018), which suggests the lobe-axis exhibited the highest initial porosity and permeability. Trends in sorting are weak in Lobe 1. Lobe off-axis deposits are generally better sorted than both lobe axis and lobe fringes, and therefore the original porosity may have been higher (Fig. 12C, D). However, as grain-size and matrix content are considered stronger controls on reservoir quality (Hirst et al., 2002; Lien et al., 2006; Porten et al., 2016), they are likely to overprint this parameter. At architectural-element scale, the sandstone-percentage and degree of amalgamation decrease away the from lobe axis to the lobe fringe (90 to 54%and 78.38 to 3.64% respectively; Figures 8D and F). This suggests lobe-axes had higher reservoir volume and connectivity. Authigenic mineral content is less variable than in the channel-fill element, but is slightly higher in lobe off-axis and lobe axis (Fig. 8D, F), suggesting increased fluid flow during diagenesis. Lobe axis deposits exhibit the best depositional reservoir quality at both grain- and architectural-scales (Fig. 10). Reservoir potential decreases slightly from lobe axis to lobe off-axis, at grain- and architectural-scale (Fig. 10). The relatively abrupt increase in matrix content, decrease in grain-size, decrease in sandstone-percentage and decrease in amalgamation from lobe off-axis to lobe fringe (over a scale of 3.25 km) suggests that depositional reservoir quality and vertical connectivity within lobes decreases considerably from the lobe off-axis to the lobe fringe (Fig. 10). Where lobe fringe successions are reservoir prospects, they are likely to be challenging due to their (relatively) finer grain-size, increased matrix content, reduced thickness and poorer connectivity compared to more proximal positions (Kane and Pontén, 2012; Marchand et al., 2015; Southern et al., 2017; Fildani et al., 2018).

7.2.4 Process controls on depositional reservoir quality distribution

Lobes exhibit lateral facies changes that reflect different sub-environments. Lobe axis deposits are dominated by high-density turbidites, lobe off-axis deposits contain a mixture of high- and low-density turbidites and lobe fringe deposits are dominated by low-density turbidites (Figs. 5, 14; e.g. Prélat et al., 2009). Lateral variation of textural properties and composition has been observed in experimental studies (e.g. Middleton, 1967; Garcia, 1994; Gladstone et al., 1998; Hodson and Alexander, 2010; Pyles et al., 2013) and in ancient deposits (Fig. 14; e.g. Hirst et al., 2002; Kane et al., 2017; Lien et al., 2006; Marchand et al., 2015; Porten et al., 2016; Southern et al., 2017; Fildani et al., 2018). Coarse grains are deposited by high-density turbidity currents in proximal positions whereas fines that reach the basin-floor are transported to distal positions in low-density turbidity currents (Fig. 14; e.g. Middleton, 1967). Enrichment of fine-grained material in the lobe fringes may be due to entrainment of substrate in the channel-lobe transition zone, and proximal lobe positions (Kane and Pontén, 2012; Fildani et al., 2018). As grain-size and matrix are strong controls on depositional reservoir quality, their segregation within flow deposits influences reservoir potential distribution within lobes (Figs. 10, 14).

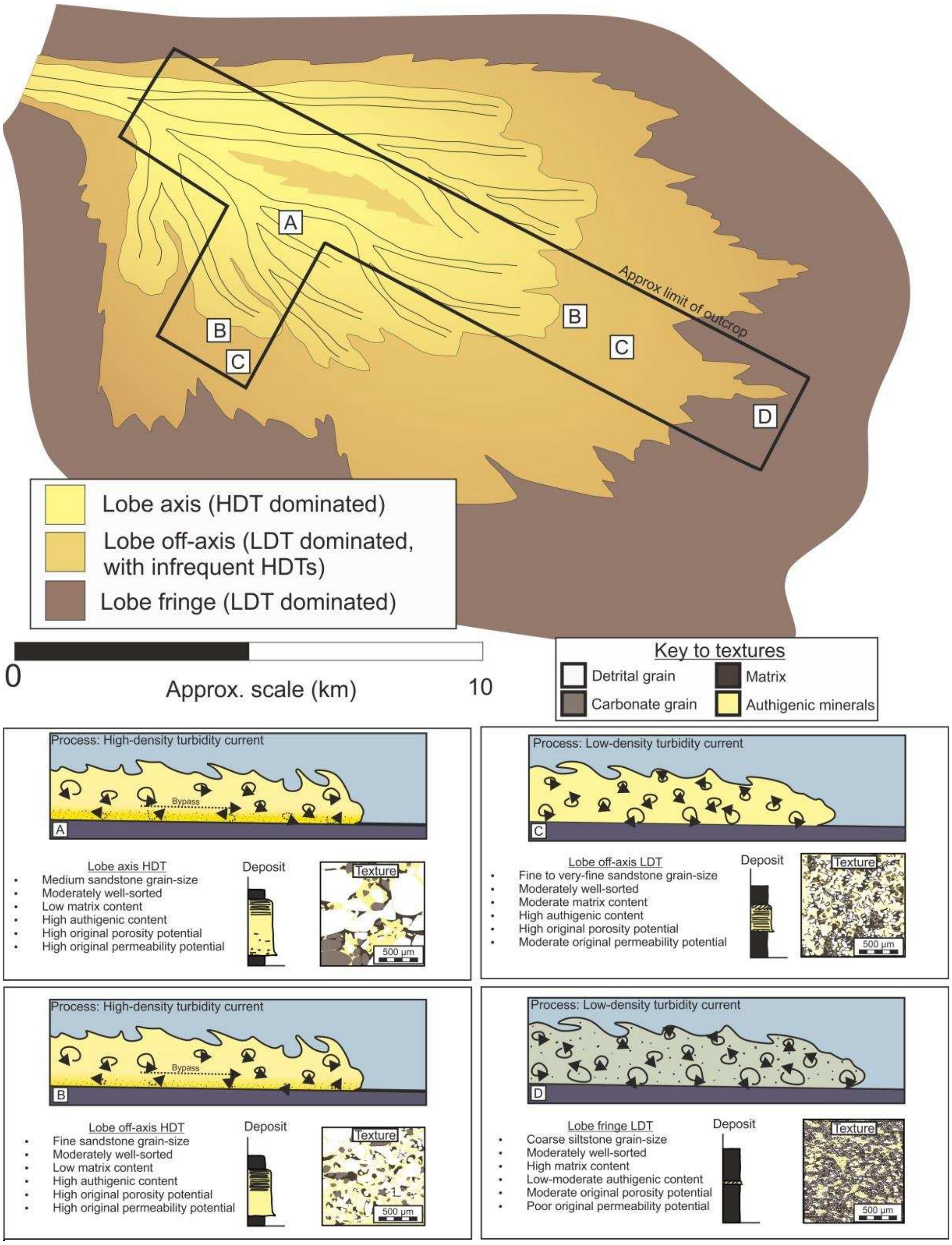

Figure 14: Illustration of flow-process controls on reservoir potential within lobes. Lobe axis deposits (A) have high reservoir potential as they are dominated by amalgamated high-density turbidites with coarse grain-sizes and low matrix content. Lobe off-axis deposits (B and C) have moderate-to-high reservoir potential as they contain a mixture of high- and low-density turbidites. Low-density turbidites have finer grain-sizes and higher amounts of matrix compared to high-density turbidites, thus reducing their reservoir potential. Lobe-fringe deposits (D) contain abundant non-amalgamated low-density

turbidites. Lobe-fringe low-density turbidites have fine grain-sizes and higher matrix content, reducing reservoir potential compared to lobe axis and lobe off-axis deposits.

7.3 Implications of detrital matrix distribution

Detrital matrix and ductile grains have a negative effect on the depositional reservoir quality by blocking pore throats (e.g. Fraser, 1935), and during compaction by forming a pseudomatrix (e.g. Marchand et al., 2015). However, clay coatings (predominantly chlorite) on grains can also act to preserve porosity and permeability by inhibiting the growth of authigenic quartz (e.g. Heald and Larese, 1974; Ehrenberg, 1993; Bloch et al., 2002; Anjos et al., 2003; Dowey et al., 2012). Authigenic quartz growth is accelerated in basins with higher heat flows (e.g. Walderhaug, 1994), such as the northern Norwegian Sea (e.g. Ritter et al., 2004). In these cases, deposits with higher matrix contents, whilst exhibiting lower initial porosity and permeability, may act to preserve the porosity and permeability present during deeper burial. Consequently, porosity and permeability in architectural element positions with lower matrix contents (e.g. lobe axis) are more likely to be reduced by authigenic quartz growth. A balance of the initial porosity and permeability, and that preserved from authigenic quartz, may favour medial values of grain-size and matrix content in these cases, such as lobe off-axis deposits. However, as temperature and compaction increase with burial the diagenetic overprint control on reservoir quality is likely to become stronger relative to the depositional control (see also: Porten et al., 2016).

8.1 Conclusions

Two deep-water architectural elements, a channel-fill element and a lobe, are characterized at grain-scale using quantitative methodology to map depositional reservoir quality spatially within individual architectural elements for the first time. Quantification of these data and their rates of change can be important parameters for sub-surface predictability and fluid flow simulation models. Textural and architectural properties show strong spatial variation in both elements. The distribution of initial depositional reservoir quality within, and between sub-environments is controlled by flow processes and their spatial and temporal evolution.

Within the channel-fill element, channel-axis deposits have the best depositional reservoir quality as they have the coarsest grain-size and lowest matrix content. However, depositional reservoir quality decreases upwards within the channel-axis, as the proportion of high-density turbidites decreases, and low-density turbidites increases as the channel-fill aggrades. Channel-margin deposits consist of low-density turbidites which have low reservoir potential due to their finer grain-sizes and high matrix content. Channel-axis deposits are also more amalgamated, and contain a greater thickness of sandstone, therefore they have better connectivity and volume compared to channel-margin deposits. Lobe axis deposits are dominated by high-density turbidites, which have better depositional reservoir quality compared to the lobe off-axis and lobe fringe as they have the coarsest grain-size, lowest matrix content, most amalgamation and highest net-to-gross. Lobe off-axis deposits contain a mixture of high- and low-density turbidites, giving moderate depositional reservoir quality. Lobe fringe deposits are characterized by low-density turbidites, which have the poorest depositional reservoir quality as they have the finest grain-size, highest matrix content, lowest degree of amalgamation and lowest net-to-gross. The rate of change in grain-size, matrix content and amalgamation increases from lobe off-axis to lobe fringe. This suggests reservoir potential decreases more abruptly from the lobe off-axis into the lobe fringe compared to from the lobe axis to lobe off-axis. However, in basin-fills with high heat-flow, sub-environments with increased detrital matrix and clay-coating of grains which inhibit authigenic quartz growth (e.g. lobe off-axis), may preserve initial porosity and permeability post-diagenesis. The studied deep-water architectural elements exhibit similar meso-scale facies, stacking patterns and lithofacies distributions to deep-water systems of different basins, ages and delivery systems. Quantified depositional reservoir quality distribution intimately ties to this predictable facies organisation and should therefore be predictable elsewhere.

Acknowledgments

The authors are grateful to the AAPG Foundation Grants-In-Aid program for the award of the R. Dana Russell memorial grant, which part-funded this research. We thank Salvatore Critelli for his editorial handling of the paper and the reviews of Salvatore Milli and an anonymous reviewer whose comments enhanced the clarity of the manuscript.

References

Aehnelt, M., Worden, R.H., Canham, A.C., Hill, S.J., Hodgson, D.M., and Flint, S.S., 2013, Geochemical correlation in an exhumed submarine channel complex (Tabernas Basin, SE Spain): Comparison to sedimentological correlation at various length scales: Journal of Sedimentary Research, v. 83, no. 8, p. 669–690, doi: 10.2110/jsr.2013.41.

Afifi, A.M., 2005, The anatomy of the world's largest oil field: AAPG Search and Discovery, v. Article 20.

Ajdukiewicz, J.M., Nicholson, P.H., and Esch, W.L., 2010, Prediction of deep reservoir quality using early diagenetic process models in the Jurassic Norphlet Formation, Gulf of Mexico: AAPG Bulletin, v. 94, no. 8, p. 1189–1227, doi: 10.1306/04211009152.

Al Ja'aidi, O.S., McCaffrey, W.D., and Kneller, B.C., 2004, Factors influencing the deposit geometry of experimental turbidity currents: implications for sand-body architecture in confined basins, *in* Lomas, S.A. and Joseph, P. eds., Confined Turbidite Systems, Geological Society, London, Special Publications, London, p. 45–58.

Allen, J.R.L., 1982, Sedimentary structures, Vol. 1-2: Elsevier, Amsterdam.

Allen, J.R.L., and Friend, P.F., 1976, Relaxation time of dunes in decelerating aqueous flows: Journal of the Geological Society, v. 132, no. 1, p. 17–26.

Anjos, S.M.C., De Ros, L.F., and Silva, C.M.A., 2003, Chlorite authigenesis and porosity preservation in the Upper Cretaceous marine sandstones of the Santos Basin, offshore eastern Brazil, *in* Worden, R., and Morad, S. eds., Clay Mineral Cements in Sandstones, Special Publcation Number 34 of the International Association of Sedimentologists, p. 291–316.

Baas, J.H., Kesteren, W.V.A.N., and Postma, G., 2004, Deposits of depletive high-density turbidity currents : a flume analogue of bed geometry , structure and texture: Sedimentology, v. 51, p. 1053–1088, doi: 10.1111/j.1365-3091.2004.00660.x.

Baas, J.H., Best, J.L., and Peakall, J., 2011, Depositional processes , bedform development and hybrid bed formation in rapidly decelerated cohesive (mud-sand) sediment flows . Sedimentology: Sedimentology, v. 58, no. July 2016, p. 1953–1987, doi: 10.1111/j.1365-3091.2011.01247.x.

Barton, M., O'Byrne, C., Pirmez, C., Prather, B., van Der Vlugt, F., Alpak, F.O., and Sylvester, Z., 2010, Turbidite channel architecture: recognizing and quantifying the distribution of channel-base drapes using core and dipmeter data, *in* Pöppelreiter, M., García-Carballido, C., and Kraaijveld, M. eds., Dipmeter and borehole image log technology, AAPG Memoir 92, p. 195–210.

Bayliss, N.J., and Pickering, K.T., 2015, Deep-marine structurally confined channelised sandy fans: Middle Eocene Morillo System, Ainsa Basin, Spanish Pyrenees: Earth Science Reviews, v. 144, p. 82–106, doi: 10.1016/j.earscirev.2014.11.014.

Beard, D.C., and Weyl, P.K., 1973, Influence of texture on porosity of unconsolidated sands: AAPG Bulletin, v. 57, no. 2, p. 349–369, doi: 10.1306/819A4272-16C5-11D7-8645000102C1865D.

Beaubouef, R.T., 2004, Deep-water leveed-channel complexes of the Cerro Toro Formation, Upper Cretaceous, southern Chile: AAPG Bulletin, v. 88, no. 11, p. 1471–1500, doi: 10.1306/06210403130.

Bell, D., Stevenson, C.J., Kane, I.A., Hodgson, D.M., and Poyatos-Moré, M. *in press*, The role of seabed topography in the development of contemporaneous but contrasting depositonal architectures in a basin-floor system: Journal of Sedimentary Research,.

Best, J.L., and Bridge, J.S., 1992, The morphology and dynamics of low amplitude bedwaves upon upper stage plane beds and the preservation of planar laminae: Sedimentology, v. 39, p. 737–752, doi: 10.1111/j.1365-3091.1992.tb02150.x.

Bloch, S., Lander, R.H., and Bonnell, L., 2002, Anomalously high porosity and permeability in deeply buried sandstone reservoirs: Origin and predictability: AAPG Bulletin, v. 86, no. 2, p. 301–328, doi: 10.1306/61EEDABC-173E-11D7-8645000102C1865D.

Caja, M.A., Marfil, R., Garcia, D., Remacha, E., Morad, S., Mansurbeg, H., Amorosi, A., Martínez-Calvo, C., and Lahoz-Beltrá, R., 2010, Provenance of siliciclastic and hybrid turbiditic arenites of the Eocene Hecho Group, Spanish Pyrenees: Implications for the tectonic evolution of a foreland basin: Basin Research, v. 22, no. 2, p. 157–180, doi: 10.1111/j.1365-2117.2009.00405.x.

Campion, K.M., Sprague, A.R., Mohrig, D., Lovell, R.W., Drzewiecki, P.A., Sullivan, M.D., Ardill, J.A., Jensen, G.N., and Sickafoose, D.K., 2000, Outcrop expression of confined channel complexes, *in* Weimar, P., Slatt, R.M., Coleman, J., Rosen, N.C., Nelson, H., Bouma, A.H., Styzen, M.J., and Lawrence, D.T. eds., Deep-Water Reservoirs of the World: SEPM, Gulf Coast Section, 20th Annual Research Conference, p. 127–151.

Cartigny, M.J.B., Eggenhuisen, J.T., Hansen, E.W.M., and Postma, G., 2013, Concentration-dependent flow stratification in experimental high-density turbidity currents and their relevence to turbidite facies models: Journal of Sedimentary Research, v. 83, p. 1046–1064, doi: 10.2110/jsr.2013.71.

Clare, M.A., Talling, P.J., Challenor, P., Malgesini, G., and Hunt, J., 2014, Distal turbidites reveal a common distribution for large (>0.1 km3) submarine landslide recurrence: Geology, v. 42, no. 3, p. 263–266.

Clark, J.D., Kenyon, N.H., and Pickering, K.T., 1992, Quantitative analysis of the geometry of submarine channels: implications for the classification of submarine fans: Geology, v. 20, no. 7, p. 633–636, doi: 10.1130/0091-7613(1992)020<0633:QAOTGO>2.3.CO.

Clark, J.D., and Pickering, K.T., 1996, Architectural elements and growth patterns of submarine channels: Application to hydrocarbon exploration: AAPG Bulletin, v. 80, p. 194–221, doi: 10.1306/64ED878C-1724-11D7-8645000102C1865D.

Clark, J.D., Puigdefàbregas, C., Castelltort, S., and Fildani, A., 2017, Propagation of Environmental Signals within Source-to-Sink Stratigraphy: *SEPM Field Trip Guidebook 13*, p. 1–63.

Dakin, N., Pickering, K.T., Mohrig, D., and Bayliss, N.J., 2013, Channel-like features created by erosive submarine debris flows: Field evidence from the Middle Eocene Ainsa Basin, Spanish Pyrenees: Marine and Petroleum Geology, v. 41, p. 62–71, doi: 10.1016/j.marpetgeo.2012.07.007.

Das Gupta, K., and Pickering, K.T., 2008, Petrography and temporal changes in petrofacies of deep-marine Ainsa – Jaca basin sandstone systems , Early and Middle Eocene , Spanish Pyrenees: Sedimentology, v. 55, no. 4, p. 1083–1114, doi: 10.1111/j.1365-3091.2007.00937.x.

Deptuck, M.E., Piper, D.J.W., Savoye, B., and Gervais, A., 2008, Dimensions and architecture of late Pleistocene submarine lobes off the northern margin of East Corsica: Sedimentology, v. 55, p. 869–898.

Di Celma, C.N., Brunt, R.L., Hodgson, D.M., Flint, S.S., and Kavanagh, J.P., 2011, Spatial and Temporal Evolution of a Permian Submarine Slope Channel-Levee System, Karoo Basin, South Africa: Journal of Sedimentary Research, v. 81, no. 8, p. 579–599, doi: 10.2110/jsr.2011.49.

Di Celma, C., Teloni, R., and Rustichelli, A., 2014, Large-scale stratigraphic architecture and sequence analysis of an early Pleistocene submarine canyon fill , Monte Ascensione succession (Peri-Adriatic basin, eastern central Italy): International Journal of Earth Sciences, v. 103, no. 3, p. 843–875, doi: 10.1007/s00531-013-0984-3.

Dickinson, W.R., 1970, Interpreting detrital modes of graywacke and arkose: Journal of Sedimentary Research, v. 40, no. 2, p. 695 LP-707.

Dowey, P.J., Hodgson, D.M., and Worden, R.H., 2012, Pre-requisites, processes, and prediction of chlorite grain coatings in petroleum reservoirs: A review of subsurface examples: Marine and Petroleum Geology, v. 32, no. 1, p. 63–75, doi: 10.1016/j.marpetgeo.2011.11.007.

Ehrenberg, S.N., 1989, Assessing the relative importance of compaction processes: AAPG Bulletin, v. 73, no. 10, p. 1274–1276.

Ehrenberg, S.N., 1993, Preservation of Anomalously High Porosity in Deeply Buried Sandstones by Grain-Coating Chlorite: Examples from the Norwegian Continental Shelf: AAPG Bulletin, v. 77, no. 7, p. 1260–1286.

Ehrenberg, S.N., 1997, Influence of depositional sand quality and diagenesis on porosity and permeability: Examples from Brent Group reservoirs, Northern North Sea: SEPM Journal of Sedimentary Research, v. 67, no. 1, p. 197–211, doi: 10.1306/D4268531-2B26-11D7-8648000102C1865D.

Emmel, F.J., and Curray, J.R., 1983, The Bengal Submarine Fan, Northeastern Indian ocean: Geo-Marine Letters, v. 3, no. 2, p. 119–124, doi: 10.1007/BF02462456.

Eschard, R., Albouy, E., Deschamps, R., Euzen, T., and Ayub, A., 2003, Downstream evolution of turbiditic channel complexes in the Pab Range outcrops (Maastrichtian, Pakistan): Marine and Petroleum Geology, v. 20, no. 6–8, p. 691–710, doi: 10.1016/j.marpetgeo.2003.02.004.

Fildani, A., Clark, J., Covault, J.A., Power, B., Romans, B.W., and Aiello, I.W., 2018, Muddy sand and sandy mud on the distal Mississippi fan: Implications for lobe depositional processes: Geosphere, v. 14, no. 3, p. 1051–1066.

Folk, R.L., and Ward, W.C., 1957, Brazos River Bar: A Study in the Significance of Grain Size Parameters: Journal of Sedimentary Petrology, v. 27, no. 1, p. 3–26.

Fontana, D., Zuffa, G.G., and Garzanti, E., 1989, The interaction of eustacy and tectonism from provenance studies of the Eocene Hecho Group Turbidite Complex (South-Central Pyrenees, Spain): Basin Research, v. 2, no. 4, p. 223–237.

Fraser, H.J., 1935, Experimental Study of the Porosity and Permeability of Clastic Sediments: The Journal of Geology, v. 43, no. 8, p. 910–1010, doi: 10.1086/624388.

Galy, V., France-Lanord, C., Beyssac, O., Faure, P., Kudrass, H., and Palhol, F., 2007, Efficient organic carbon burial in the Bengal fan sustained by the Himalayan erosional system: Nature, v. 450, p. 407.

Garcia, M., 1994, Depositional turbidity currents laden with poolry sorted sediment: Journal of Hydraulic Engineering, v. 120, no. 11, p. 1240–1263.

Gardner, M.H., and Borer, J.M., 2000, Submarine channel architecture along a slope to basin profile, Brushy Canyon Formation, West Texas, *in* Bouma, A.H. and Stone, C.G. eds., Fine-Grained Turbidite Systems: AAPG Memoir 72 and SEPM Special Publication 68, p. 195–214.

Gazzi, P., 1966, Le Arenarie del flysch sopracretaceo dell'Appennino modenese; correlazioni con il flysch di Monghidoro: Mineralogica e Petrografica Acta, v. 16, p. 69–97.

Gladstone, C., Phillips, J.C., and Sparks, R.S.J., 1998, Experiments on bidisperse, constant volume gravity currents: propagation and sediment deposition: Sedimentology, v. 45, p. 833–843.

Grundvåg, S.A., Johannessen, E.P., Helland-Hansen, W., and Plink-Björklund, P., 2014, Depositional architecture and evolution of progradationally stacked lobe complexes in the Eocene Central Basin of Spitsbergen: Sedimentology, v. 61, no. 2, p. 535–569, doi: 10.1111/sed.12067.

Gwiazda, R., Paull, C.K., Ussler, W., and Alexander, C.R., 2015, Evidence of modern fine-grained sediment accumulation in the Monterey Fan from measurements of the pesticide DDT and its metabolites: Marine Geology, v. 363, p. 125–133, doi: https://doi.org/10.1016/j.margeo.2015.02.006.

Haile, B.G., Klausen, T.G., Czarniecka, U., Xi, K., Jahren, J., and Hellevang, H., 2017, How are diagenesis and reservoir quality linked to depositional facies? A deltaic succession, Edgeøya, Svalbard: Marine and Petroleum Geology, v. 92, 519-546 doi: https://doi.org/10.1016/j.marpetgeo.2017.11.019.

Hardage, B.A., Carr, D.L., Lancaster, D.E., Simmons, J.L., Elphick, R.Y., Pendleton, V.M., and Johns, R.A., 1996, 3-D seismic evidence of the effects of carbonate karst collapse on overlying clastic stratigraphy and reservoir compartmentalization: Geophysics, v. 61, no. 5, p. 1336–1350, doi: 10.1190/1.1444057.

Heald, M.T., and Larese, R.E., 1974, Influence of coatings on quartz cementation: Journal of Sedimentary Research, v. 44, no. 4.

Hirst, J.P.P., Benbakir, A., Payne, D.F., and Westlake, I.R., 2002, Tunnel valleys and density flow processes in the Upper Ordovician glacial succession, Illizi Basin, Algeria: Influence on reservoir quality: Journal of Petroleum Geology, v. 25, no. 3, p. 297–324, doi: 10.1111/j.1747-5457.2002.tb00011.x.

Hiscott, R.N., Hall, F.R., and Pirmez, C., 1997, Turbidity-current overspill from the Amazon channel: texture of the silt/sand load, paleoflow from anisotropy of magnetic susceptibility and implications for flow processes, *in* Flood, R.D., Piper, D.J.W., Klaus, A., and Peterson, L.C. eds., Proceedings of the Ocean Drilling Program, Scientific Results, Ocean Drilling Program, College Station, Texas, p. 53–78.

Hodgson, D.M., 2009, Distribution and origin of hybrid beds in sand-rich submarine fans of the Tanqua depocentre, Karoo Basin, South Africa: Marine and Petroleum Geology, v. 26, no. 10, p. 1940–1956, doi: 10.1016/j.marpetgeo.2009.02.011.

Hodgson, D. M., Kane, I. A., Flint, S. S., Brunt, R. L., & Ortiz-Karpf, A. (2016). Time-transgressive confinement on the slope and the progradation of basin-floor fans: Implications for the sequence stratigraphy of deep-water deposits. Journal of Sedimentary Research, 86, no. 1, 73-86, doi: 10.2110/jsr.2016.3

Hodson, J.M., and Alexander, J., 2010, The Effects of Grain-Density Variation on Turbidity Currents and Some Implications for the Deposition of Carbonate Turbidites: Journal of Sedimentary Research, v. 80, no. 6, p. 515–528, doi: 10.2110/jsr.2010.051.

Hubbard, S.M., Covault, J.A., Fildani, A., and Romans, B.W., 2014, Sediment transfer and deposition in slope channels: Deciphering the record of enigmatic deep-sea processes from outcrop: Bulletin of the Geological Society of America, v. 126, no. 5–6, p. 857–871, doi: 10.1130/B30996.1.

Ingersoll, R. V, Bullard, T.F., Ford, R.L., Grimm, J.P., Pickle, J.D., and Sares, S.W., 1984, The effect of grain size on detrital modes: a test of the Gazzi-Dickinson point-counting method: Journal of Sedimentary Research, v. 54, no. 1, p. 103–116.

Jolley, S.J., Fisher, Q.J., and Ainsworth, R.B., 2010, Reservoir compartmentalization: an introduction: Geological Society, London, Special Publications, v. 347, no. 1, p. 1 LP-8.

Kane, I.A., and Pontén, A.S.M., 2012, Submarine transitional flow deposits in the Paleogene Gulf of Mexico: Geology, v. 40, no. 12, p. 1119–1122, doi: 10.1130/G33410.1.

Kane, I.A., Pontén, A.S.M., Vangdal, B., Eggenhuisen, J.T., Hodgson, D.M., and Spychala, Y.T., 2017, The stratigraphic record and processes of turbidity current transformation across deep-marine lobes: Sedimentology, doi: 10.1111/SED.12346.

Kerr, D.R., and Jirik, L.A., 1990, Fluvial architecture and reservoir compartmentalization in the Oligocene Middle Frio Formation of South Texas: AAPG Bulletin, v. 74, p. 373–380, doi: 10.1306/20B2311F-170D-11D7-8645000102C1865D.

Kilhams, B., Hartley, A., Huuse, M., and Davis, C., 2015, Characterizing the Paleocene turbidites of the North Sea : Maureen Formation, UK Central Graben, *in* Mckie, T., Rose, P.T.S., Hartley, A., Jones, D.W., and Armstrong, T.L. eds., Tertiary Deep-Marine Reservoirs of the North Sea Reservoirs of the North Sea Region, Geological Society, London, p. 43–62.

Kilhams, B., Hartley, A., Huuse, M., and Davis, C., 2012, Characterizing the Paleocene turbidites of the North Sea: the Mey Sandstone Member, Lista Formation, UK Central Graben: Petroleum Geoscience, v. 18, p. 337–354, doi: 10.1144/SP403.1.

Labaume, P., Mutti, E., and Seguret, M., 1987, Megaturbidites : A Depositional Model From the Eocene: Geo-Marine Letters, v. 7, no. 2, p. 91–101.

Labaume, P., Séguret, M., and Seyve, C., 1985, Evolution of a turbiditic foreland basin and analogy with an accretionary prism: Example of the Eocene South-Pyrenean Basin: Tectonics, v. 4, no. 7, p. 661, doi: 10.1029/TC004i007p00661.

Lan, C., Yang, M., and Zhang, Y., 2016, Impact of sequence stratigraphy, depositional facies and diagenesis on reservoir quality: A case study on the Pennsylvanian Taiyuan sandstones, northeastern Ordos Basin, China: Marine and Petroleum Geology, v. 69, p. 216–230, doi: 10.1016/j.marpetgeo.2015.09.009.

Li, P., Kneller, B.C., Hansen, L., and Kane, I.A., 2016, The classical turbidite outcrop at San Clemente, California revisited: An example of sandy submarine channels with asymmetric facies architecture: Sedimentary Geology, v. 346, p. 1–16, doi:

10.1016/j.sedgeo.2016.10.001.

Lien, T., Midtbø, R.E., and Martinsen, O.J., 2006, Depositional facies and reservoir quality of deep-marine sandstones in the Norwegian Sea: Norwegian Journal of Geology, v. 86, no. 2, p. 71–92

Lowe, D.R., 1982, Sediment Gravity Flows: II Depositional Models with Special Reference to the Deposits of High-Density Turbidity Currents: Journal of Sedimentary Research, v. 52, no. 1.

Marchand, A.M.E., Apps, G., Li, W., and Rotzien, J.R., 2015, Depositional processes and impact on reservoir quality in deepwater Paleogene reservoirs, US Gulf of Mexico: AAPG Bulletin, v. 99, no. 9, p. 1635–1648, doi: 10.1306/04091514189.

Marini, M., Milli, S., Ravnås, R., and Moscatelli, M., 2015, A comparative study of confined vs. semi-confined turbidite lobes from the Lower Messinian Laga Basin (Central Apennines, Italy): implications for assesment of reservoir architecture: Marine and Petroleum Geology, v. 63, p. 142–165, doi: 10.1016/j.marpetgeo.2015.02.015.

Marzano, M.S., 1988, Controls on permeability for unconsolidated sands from conventional core data offshore Gulf of Mexico: AAPG bulletin, v. 38, p. 113–120.

McHargue, T., Pyrcz, M.J., Sullivan, M.D., Clark, J.D., Fildani, A., Romans, B.W., Covault, J.A., Levy, M., Posamentier, H.W., and Drinkwater, N.J., 2011, Architecture of turbidite channel systems on the continental slope: Patterns and predictions: Marine and Petroleum Geology, v. 28, no. 3, p. 728–743, doi: 10.1016/j.marpetgeo.2010.07.008.

McKie, T., Rose, P.T.S., Hartley, A.J., Jones, D.W., and Armstrong, T.L., 2015, Tertiary deep-marine reservoirs of the North Sea region: an introduction, *in* McKie, T., Rose, P.T.S., Hartley, A.J., Jones, D.W., and Armstrong, T.L. eds., Tertiary Deep-Marine Reservoirs of the North Sea Reservoirs of the North Sea, The Geological Society of London, p. 403.

Miall, A.D., 1985, Architectural-Element Analysis: A New Method of Facies Analysis Applied to Fluvial Deposits: Earth-Science Reviews, v. 22, no. 4, p. 261–308.

Middleton, G. V., 1967, Experiments on density and turbidity currents: III. Deposition of sediment: Canadian Journal of Earth Sciences, v. 4, no. 3, p. 475–505, doi: 10.1139/e67-025.

Moody, J.D., Pyles, D.R., Clark, J., and Bouroullec, R., 2012, Quantitative outcrop characterization of an analog to weakly confined submarine channel systems: Morillo 1 member, Ainsa Basin, Spain: AAPG Bulletin, v. 96, no. 10, p. 1813–1841, doi: 10.1306/01061211072.

Muñoz, J.A., 1992, Evolution of a continental collision belt: ECORS-Pyrenees crustal balanced cross-section, *in* McClay, K.R. ed., Thrust Tectonics, Springer Netherlands, Dordrecht, p. 235–246.

Mutti, E., 1977, Distinctive thin-bedded turbidite facies and related depositional environments in the Eocene Hecho Group (South-central Pyrenees, Spain): Sedimentology, v. 24, no. 1, p. 107–131, doi: 10.1111/j.1365-3091.1977.tb00122.x.

Mutti, E., 1984, The Hecho Eocene submarine fan system, south-central Pyrenees, Spain: Geo-Marine Letters, v. 3, no. 2–4, p. 199–202, doi: 10.1007/BF02462468.

Mutti, E., 1985, Turbidite Systems and Their Relations to Depositional Sequences, *in* Zuffa, G.G. ed., Provenance of Arenites, Reidel Publishing Co., Dordrecht, p. 65–93.

Mutti, E., 1992, Turbidite Sandstones: Agip, Istituto di Geologia Università di Parma, Milan.

Mutti, E., and Ricci-Lucchi, F., 1972, Le torbiditi dell'Appennino settentrionale: introduzioni all'analisi di facies: Mem. Soc. Geol. Ital., v. 11/2, p. 161–199, doi: -.

Mutti, E., and Normark, W.R., 1987, Comparing Examples of Modern and Ancient Turbidite Systems: Problems and Concepts, *in* Leggett, J.K. and Zuffa, G.G. eds., Marine clastic sedimentology, Springer Netherlands, Dordrecht, p. 1–38.

Mutti, E., Séguret, M., and Sgavetti, M., 1988, Sedimentation and deformation in the Tertiary Sequences of the Southern Pyrenees: Field trip 7: University of Parma.

Nardin, T.R., Hein, F.J., Gorsline, D.S., and Edwards, B., 1979, A Review of mass movement processes, sediment and acoustic characteristics, and contrasts in slope and base-of-slope systems versus canyon-fan-basin floor systems: SEPM Special Publications, , no. 27, p. 61–73.

Njoku, C., and Pirmez, C., 2011, Sedimentary Controls on Porosity and Permeability in Deepwater Turbidites: Nigeria Annual International Conference and Exhibition, p. 1–5, doi: 10.2118/150805-ms.

Payros, A., Pujalte, V., and Orue-Etxebarria, X., 1999, The South Pyrenean Eocene carbonate megabreccias revisited: New interpretation based on evidence from the Pamplona Basin: Sedimentary Geology, v. 125, no. 3, p. 165–194, doi: 10.1016/S0037-0738(99)00004-4.

Pettijohn, F.J., Potter, P.E., and Siever, R., 1972, Sand and Sandstone: Springer, Berlin-Herdelberg-New York. p. 1-553

Pettingill, H.S., 1998, Turbidite plays' immaturity means big potential remains: Oil & Gas Journal, v. 96, no. 40, p. 106–111

Pickering, K.T., and Corregidor, J., 2005, Mass-transport complexes, (MTCs) and tectonic control on basin-floor submarine fans, middle eocene, south Spanish Pyrenees: Journal of Sedimentary Research, v. 75, no. 5, p. 761–783, doi: 10.2110/jsr.2005.062.

Piper, D., Cochonat, P., and Morrison, M.L., 1999, The sequence of events around the epicentre of the 1929 Grand Banks earthquake: Initiation of debris flows and turbidity current inferred from sidescan sonar: Sedimentology, v. 46, p. 79–97, doi: 10.1046/j.1365-3091.1999.00204.x.

Pittman, E.D., and Larese, R.E., 1991, Compaction of Lithic Sands: Experimental Results and Applications (1): AAPG Bulletin, v. 75, no. 8, p. 1279–1299.

Porten, K.W., Kane, I.A., Warchol, M., and Southern, S.J., 2016, Depositional reservoir quality of deep-marine sandstones: A sedimentolgical process-based approach - an example from the Springrar Formation, North-Western Vøring Basin, Norwegian Sea: Journal of Sedimentary Research, v. 86, no. 11, p. 1269–1286.

Prélat, A., Hodgson, D.M., and Flint, S.S., 2009, Evolution, architecture and hierarchy of distributary deep-water deposits: a high-resolution outcrop investigation from the Permian Karoo Basin, South Africa: Sedimentology, v. 56, no. 7, p. 2132–2154, doi: 10.1111/j.1365-3091.2009.01073.x.

Prélat, A., Covault, J.A., Hodgson, D.M., Fildani, A., and Flint, S.S., 2010, Intrinsic controls on the range of volumes, morphologies, and dimensions of submarine lobes: Sedimentary Geology, v. 232, no. 1, p. 66–76, doi: 10.1016/j.sedgeo.2010.09.010.

Pryor, W.A., 1973, Permeability-porosity patterns and variations in some Holocene sand bodies: AAPG Bulletin, v. 57, no. 1, p. 162–189, doi: 10.1306/819A4252-16C5-11D7-8645000102C1865D.

Puigdefàbregas, C., Rupke, N.A., and Sedo, J.S., 1975, The sedimentary evolution of the Jaca Basin, *in* The Sedimentary Evolution of the Palaeogene South Pyrenean Basin.

Pyles, D.R., Straub, K.M., and Stammer, J.G., 2013, Spatial variations in the composition of turbidites due to hydrodynamic fractionation: Geophysical Research Letters, v. 40, no. August 2013, p. 3919–3923, doi: 10.1002/grl.50767.

Ramm, M., and Bjørlykke, K., 1994, Porosity/depth trends in reservoir sandstones: Assessing the quantitative effects of varying pore-pressure, temperature history and mineralogy, Norwegian Shelf data: Clay Minerals, v. 29, p. 475–490.

Remacha, E., and Fernández, L.P., 2003, High-resolution correlation patterns in the turbidite systems of the Hecho Group (South-Central Pyrenees, Spain): Marine and Petroleum Geology, v. 20, no. 6, p. 711–726, doi: 10.1016/j.marpetgeo.2003.09.003.

Remacha, E., Gual, G., Bolaño, F., Arcuri, M., Oms, O., Climent, F., Crumeyrolle, P., Fernández, L.P., Vicente, J.C., and Suarez, J., 2003, Sand-rich turbidite systems of the Hecho Group from slope to basin plain; facies, stacking patterns, controlling factors and diagnostic features: American Association of Petroleum Geologists, International Conference and Exhibition, Barcelona, Spain, September 21–24. *Geological field trip 12*, *South-Central Pyrenees*.

Remacha, E., Fernández, L.P., and Maestro, E., 2005, The Transition Between sheet-like lobe and basin-plain turbidites in the Hecho Basin (South-Central Pyrenees, Spain): Journal of Sedimentary Research, v. 75, no. 5, p. 798–819, doi: 10.2110/jsr.2005.064.

Ritter, U., Zielinski, G.W., Weiss, H.M., Zielinski, R.L.B., and Sættem, J., 2004, Heat flow in the Vøring Basin , Mid-Norwegian Shelf: Petroleum Geoscience, v. 10, no. 4, p. 353–365, doi: https://doi.org/10.1144/1354-079303-616.

Rosell, J., and Wiezorek, J., 1989, Main features of megaturbidites in the Eocene of southern Pyrenees: Annales Societatis Geologorum Poloniae, v. 59, p. 3–16.

Ruffell, A.H., Moles, N.R., and Parnell, J., 1998, Characterisation and prediction of sediment-hosted ore deposits using sequence stratigraphy: Ore Geology Reviews, v. 12, no. 4, p. 207–223, doi: https://doi.org/10.1016/S0169-1368(97)00029-2.

Rupke, N.A., 1976, Sedimentology of very thick calcarenite-marlstone beds in a flysch succession, southwestern Pyrenees: Sedimentology, v. 23, p. 213–265, doi: 10.1111/j.1365-3091.1976.tb00038.x.

Saller, A., Werner, K., Sugiaman, F., Cebastiant, A., May, R., Glenn, D., and Barker, C., 2008, Characteristics of Pleistocene deep-water fan lobes and their application to an upper

Miocene reservoir model, offshore East Kalimantan, Indonesia: AAPG Bulletin, v. 92, no. 7, p. 919–949, doi: 10.1306/03310807110.

Sanders, J.E., 1965, Primary sedimentary structures formed by turbidity currents and related resuspension mechanisms, *in* Middleton, G.V. ed., Primary Sedimentary Structures and their Hydrodynamic Interpretation, SEPM Special Publication, p. 192–219.

Southard, J.B., 1991, Experimental Determination of Bed-Form Stability: Annual Review of Earth and Planetary Sciences, v. 19, no. 1, p. 423–455, doi: 10.1146/annurev.ea.19.050191.002231.

Southern, S.J., Kane, I.A., Warchoł, M.J., Porten, K.W., and McCaffrey, W.D., 2017, Hybrid event beds dominated by transitional-flow facies: Character, distribution and significance in the maastrichtian springar formation, north-west vøring basin, Norwegian Sea: Sedimentology, v. 64, no. 3, p. 747–776, doi: 10.1111/sed.12323.

Sprague, A.R., Sullivan, M.D., Campion, K.M., Jensen, G.N., Goulding, F.J., Garfield, T.R., Sickafoose, D.K., Rossen, C., and Jeannette, D.C., 2002, The physical stratigraphy of deep-water strata: A hierarchical approach to the analysis of genetically-related stratigraphic elements for improved reservoir prediction, *in* National AAPG/SEPM meeting abstracts, Houston, Texas, p. 10–13.

Spychala, Y.T., Hodgson, D.M., Prélat, A., Kane, I.A., Flint, S.S., and Mountney, N.P., 2017a, Frontal and lateral submarine lobe fringes: Comparing facies, architecture and flow processes: Journal of Sedimentary Research, v. 87, no. January, p. 1–21.

Spychala, Y.T., Hodgson, D.M., and Stevenson, C.J., 2017b, Aggradational lobe fringes : The influence of subtle intrabasinal seabed topography on sediment gravity flow processes and lobe stacking patterns: Sedimentology, v. 64, p. 582–608, doi: 10.1111/sed.12315.

Stalder, N.F., Fellin, M.G., Caracciolo, L., Guillong, M., Winkler, W., Milli, S., Moscatelli, M., and Critelli, S., 2017, Dispersal pathways in the early Messinian Adriatic foreland and provenance of the Laga Formation (Central Apennines, Italy): Sedimentary Geology, doi: https://doi.org/10.1016/j.sedgeo.2017.09.016.

Stevenson, C.J., Talling, P.J., Masson, D.G., Sumner, E.J., Frenz, M., and Wynn, R.B., 2014a, The spatial and temporal distribution of grain-size breaks in turbidites: Sedimentology, v. 61, p. 1120–1156, doi: 10.1111/sed.12091.

Stevenson, C.J., Talling, P.J., Sumner, E.J., Masson, D.G., Frenz, M., and Wynn, R., 2014b, On how thin submarine flows transported large volumes of sand for hundreds of kilometres across a flat basin plain without eroding the sea floor: Sedimentology, p. n/a-n/a, doi: 10.1111/sed.12125.

Stevenson, C.J., Jackson, C.A.-L., Hodgson, D.M., Hubbard, S.M., and Eggenhuisen, J.T., 2015, Deep-water sediment bypass: Journal of Sedimentary Research, v. 85, p. 1058–1081, doi: 10.2110/jsr.2015.63.

Sullivan, M.D., Jensen, G.N., Goulding, F.J., Jennette, D.C., Foreman, J.L., and Stern, D., 2000, Architectural analysis of deep-water outcrops: Implications for exploration and development of the Diana sub-basin, western Gulf of Mexico, *in* Weimer, P., Slatt, R.M., Bouma, A.H., and Lawrence, D.T. eds., Deep-water reservoirs of the world, Gulf Coast Section SEPM Foundation, Twentieth Annual Research Conference, p. 1010–1032.

Sumner, E.J., Amy, L.A., and Talling, P.J., 2008, Deposit Structure and Processes of Sand Deposition from Decelerating Sediment Suspensions: Journal of Sedimentary Research, v. 78, no. 8, p. 529–547, doi: 10.2110/jsr.2008.062.

Sumner, E.J., Talling, P.J., Amy, L.A., Wynn, R.B., Stevenson, C.J., and Frenz, M., 2012, Facies architecture of individual basin-plain turbidites: Comparison with existing models and implications for flow processes: Sedimentology, v. 59, p. 1850–1887, doi: 10.1111/j.1365-3091.2012.01329.x.

Talling, P.J., Wynn, R.B., Masson, D.G., Frenz, M., Cronin, B.T., Schiebel, R., Akhmetzhanov, A.M., Dallmeier-Tiessen, S., Benetti, S., Weaver, P.P.E., Georgiopoulou, A., Zühlsdorff, C., and Amy, L.A., 2007, Onset of submarine debris flow deposition far from original giant landslide.: Nature, v. 450, no. November, p. 541–544, doi: 10.1038/nature06313.

Talling, P.J., Masson, D.G., Sumner, E.J., and Malgesini, G., 2012, Subaqueous sediment density flows: Depositional processes and deposit types: Sedimentology, v. 59, p. 1937–2003, doi: 10.1111/j.1365-3091.2012.01353.x.

Teixell, A., and García-Sansegundo, J., 1995, Estructura del sector central de la Cuenca de Jaca (Pirineos meridionales): Rev. Soc. Geol. España, v. 8, no. 3, p. 215–228.

Walderhaug, O., 1994, Precipitation rates for quartz cement in sandstones determined by fluid-inclusion microthermometry and temperature-history modeling: Journal of Sedimentary Research, v. A64, no. 2, p. 324–333.

Walker, R.G., 1975, Generalized facies models for resedimented conglomerates of turbidite association: Geological Society of America Bulletin, v. 86, no. 6, p. 737–748.

Weimer, P., Slatt, R.M., Dromgoole, P., Bowman, M., and Leonard, A., 2000, Developing and Managing Turbidite Reservoirs : Case Histories and Experiences : Results of the 1998 EAGE/AAPG Research Conference 1: AAPG Bulletin, v. 84, no. 4, p. 453–465.

Wilson, M.D., 1992, Inherited grain-rimming clays in sandstones from eolian and shelf environments: their origin and control on reservoir properties, *in* Origin Diagenesis and Petrophysics of Clay Minerals in Sandstones, SEPM Special Publication No. 47, p. 209–225.

Worden, R.H., Mayall, M., and Evans, I.J., 2000, The Effect of Ductile-Lithic Sand Grains and Quartz Cement on Porosity and Permeability in Oligocene and Lower Miocene Clastics , South China Sea : Prediction of Reservoir Quality 1: AAPG Bulletin, v. 84, no. 3, p. 345–359.

Zuffa, G.G., Cibin, U., and Di Giulio, A., 1995, Arenite petrography in sequence stratigraphy:

The Journal of Geology, v. 103, no. 4, p. 451–459.